Seismic Resonant Metamaterials for the protection of an elastic-plastic SDOF system against vertically propagating seismic shear waves (SH) in nonlinear soil

by

Constantinos Kanellopoulos[1], Nikolaos Psycharis[1], Han Yang[2], Boris Jeremić[2], Ioannis Anastasopoulos[1], Božidar Stojadinović[1]

Abstract

The paper explores the key mechanisms that govern the dynamic interaction between resonant metamaterials (consisting of multiple unit cells embedded in the soil, with horizontally vibrating internal masses) and an existing nonlinear structure on nonlinear soil. Elastic behavior of the soil and of the SDOF system, representing the structure, is also investigated for deeper insights. Employing the Real-ESSI Simulator, 2D finite element (FE) models are developed and used to conduct an extensive parametric analysis, evaluating the influence of key parameters on the protective efficiency of resonant metamaterials. Both artificial and real motions are used as seismic excitation, vertically propagated through the soil as shear waves (SH), employing the Domain Reduction Method (DRM). Two protective mechanisms are identified. The first one is related to the inertial interaction of the metamaterials with the surrounding soil: out-of-phase resonant oscillation of internal masses with respect to the soil at periods close to the natural period of the structure. The maximum reduction in structural response is achieved when the resonant period of the metamaterials is equal or a bit larger than the effective period of the structure. The second mechanism is related to the kinematic interaction of the metamaterials with the surrounding soil: the presence of empty unit cells (no vibrating masses) in the soil next to the structure creates a protective “shadow” zone. This kinematic interaction mechanism becomes effective when the wavelength of the incoming seismic waves is comparable to the embedment depth of the metamaterials, and at the same time, the period of the waves is close to the natural period of the structure. When both soil and structural nonlinearities are considered, the effect of metamaterials is always beneficial, and their action is localized, making them practically harmless for neighboring structures.

1. Introduction

The concept of wave screening to protect existing structures from the incoming seismic waves is not new. It was Barkan in 1962 [1], who first reviewed several applications of trenches and sheet-pile barriers for seismic protection of structures, pointing out the knowledge gap that existed at that time on how surface seismic waves propagate in the presence of a barrier. To fill this gap, Woods [2] in 1968 and Segol et al. [3] ten years later, conducted field tests and developed numerical models, respectively, to evaluate the efficiency of trench barriers in screening elastic surface waves. Both highlighted the significance of the ratio between the depth of the barrier and the wavelength of the propagating waves compared to other parameters studied (e.g., trench width and shape). The increase of the trench depth was found to improve its effectiveness. Later, in 1983, Aviles et al. [4] investigated theoretically the use of rigid piles as barriers for elastic seismic waves, showing good results for wavelength of the incident wavefield between two and eight times the pile radius. While these were pioneering applications in the area of today’s seismic metamaterials, they do have limitations. They focus mainly on surface seismic waves, but do not consider

[1] Department of Civil, Environmental and Geomatic Engineering, ETH Zürich, Zurich, 8093, Switzerland
[2] Department of Civil and Environmental Engineering, University of California Davis, Davis, 95616, USA

the (almost) vertically propagating shear waves that excite the structures from below. In addition, large depths and pile diameters (on the order of the seismic wavelength) are required for open trenches and rigid pile barriers, respectively, to be efficient (even for reasonably high frequency seismic waves). Thus, practical construction difficulties arise, especially for soft soils and high water-table levels.

The advent of metamaterials opened the way towards controlling different kinds of waves across the entire frequency spectrum, from very high-frequency electromagnetic waves to low-frequency stress waves, such as seismic waves. In 2006, Pendry et al. [5] published a seminal article on the control of electromagnetic fields using metamaterials. Since then, in different scientific fields, such as optics [6] and acoustics [7], researchers have successfully applied the concept of metamaterials to control the wave propagation both in terms of wave attenuation and wave guiding [8].

In civil engineering, research has mainly focused on resonant metamaterials to mitigate the effects of ground-borne vibrations and seismic waves on structures. Resonant metamaterials are usually artificially made structures, that exploit the vibration of multiple masses to produce frequency bandgaps, that is, prevent wave propagation in a certain range of frequencies, close to the resonant frequency of the vibrating masses. A remarkable study on inhibiting the propagation of surface Rayleigh waves was conducted by Colombi et al. [9]. They illustrated how vertically oscillating trees (modelled numerically as a vertical array of resonators) can behave as resonant metamaterials, creating bandgaps close to their longitudinal vibration frequency (~30 Hz). By using a graded vertical array of resonators (trees in a row, of gradually increasing or decreasing height), Colombi et al. [10] showed that a broadband range of protected frequencies is feasible. A large-scale physical experiment [11], conducted in a pine-tree forest, indicated that a dense collection of trees behaves as a sub-wavelength coupled resonator, qualitatively validating the previous numerical results.

For the lower frequency seismic waves (< 10 Hz), resonant metamaterials could be used to enhance the seismic performance of structures in two ways: (a) installing them at the foundation level (meta-foundations); or (b) inside the soil next to the structure (meta-barrier). A considerate amount of work on meta-foundations has been performed on the seismic protection of fuel storage tanks from both horizontal [12–14] and vertical [15] ground motions, using periodic locally resonant meta-foundations. The influence of soil-structure interaction (SSI) in their efficiency was also investigated [16], showing beneficial effects. Obviously, implementing such a solution to an existing structure can be challenging, both in economic and construction terms, limiting its use to new structures. On the other hand, in case of meta-barriers, the resonant metamaterials are embedded into the soil next to the structure to form an array of unit cells with inner vibrating masses. Using numerical and experimental approaches [17–19], such meta-structures have been shown to be able to couple with the incoming surface waves and scatter a significant part backwards or downwards into deeper soil layers.

Graded-mass metamaterial concepts (i.e., vibrating unit cells with multiple frequencies) have also been investigated [20,21] and have been shown to extend the effective frequency bandgap range of metamaterials and, consequently, offer more broadband solutions. A potential drawback of the meta-barrier approach was shown by Zaccherini et al. [22]. It was shown that in the more realistic case of inhomogeneous soil layers with depth-increasing stiffness, the initially downward-transmitted surface waves will eventually bend upwards and travel back towards the ground surface. This implies that the successfully diverted surface waves (aiming to protect one structure) may cause additional damage to neighbouring structures. In addition, most studies have used surface waves as excitation, and only very few of them consider the most critical wave component: the body shear waves.

Colombi et al. [21] showed the potential efficiency of resonant metamaterials against both surface and body waves using *elastic* 3D finite element (FE) models. A similar concept (in terms of the protective mechanism that governs the problem) was explored by Cacciola et al. [23]. The so-called Vibrating Barrier (ViBa) was introduced, which is a large horizontally-vibrating mass inside a box buried into the soil, capable of absorbing a significant part of the energy coming from the ground motion. Indeed, part of the incoming seismic energy is used for the oscillation of the vibrating mass or dissipated by the inherent damping mechanisms of the barrier, but as it will be shown later on, energy absorption is not the main protective mechanism of such systems.

The aforementioned studies indicate that resonant metamaterials have the potential to provide effective seismic protection for new and existing structures. However, there are still many questions to be addressed before such innovative solutions can find their way into practice. Key issues that need to be addressed include: (a) the effect of the unavoidable soil and structural nonlinearities on metamaterial efficiency; (b) the impact of the vibrating masses to nearby structures; and (c) the response of metamaterials and different types of structures to more realistic seismic wave fields. In this context, this study explores the seismic performance of horizontally-vibrating resonant metamaterials, in protecting structures subjected to vertically-propagating shear waves, accounting for the nonlinear response of the soil and of the structure. A large set of elastic and inelastic numerical parametric analyses are conducted, aiming to derive deeper understanding of the governing mechanisms for seismic protection of structures using metamaterials, and to evaluate the effect of each parameter on the efficiency of the examined seismic risk mitigation method.

2. Description of the Finite Element Model

2D FE models (such as the one illustrated in **Fig. 1**) are developed to study the interaction between resonant unit cell metamaterials embedded into the soil, with an adjacent single-degree-of-freedom (SDOF) system that represents the structure. The geometry and the mesh of the model are created using the open source FE mesh generator Gmsh [24]. The simulations are performed using the Real-ESSI Simulator [25] (http://real-essi.info), which is a high fidelity finite element software package, specifically developed for realistic modelling and simulation of earthquakes, soils, structures and their dynamic interactions in the time domain.

2.1 The Domain Reduction Method (DRM)

The Domain Reduction Method (DRM) is one of the most powerful and realistic approaches to insert the seismic wave field (comprising both body and surface waves) into an FE model. Initially developed by Bielak et al. [26] and verified in the companion paper by Yoshimura et al. [27] in 2003, the DRM is implemented in the Real-ESSI Simulator. Although the DRM is still not widely used in practice, lately it has gained ground within the research community [28–32]. As implied by its name, the objective of DRM is to reduce a large computational domain (including the seismic source, wave propagation through rock and soil layers, and the structure of interest) to a much smaller domain (including only local soil and the structure of interest), allowing realistic modelling of a seismic event with the same accuracy, but with orders of magnitude less computational cost. This can be achieved by breaking down the original problem in two steps, the first one dealing with the propagation of seismic waves in a large auxiliary free-field domain that comprises all problem components (seismic source, rock and soil layers) with the exception of the structure(s) of interest, and the second one focusing on the main part of the problem, modelled with a reduced domain that encompasses the local soil and the structure(s) of interest.

The purpose of the first step is to generate the motions that will be used in the second step as input for the main model. Thus, during the first step, the displacement and acceleration time histories of the nodes that lie on the elements at the boundary of the two domains (so-called DRM elements, **Fig. 1**) are recorded. Knowing these nodal time histories makes it possible to apply the so-called effective forces P^{eff} on the DRM elements of the reduced domain, that will produce the exact same seismic wave field as in the larger auxiliary domain. It is important to clarify that this will be exactly the case when the main model is a free-field model. If a structure is present, the seismic wave field will be modified accordingly. The extra waves generated from the oscillation of the structure could be trapped inside the domain and interfere with the results. This can be avoided by adding an extra layer of so-called damping elements (**Fig. 1**), with progressively higher damping ratios. In this study, a constant Rayleigh damping ratio of 40% is used for all damping elements, as it was found to yield the same results with progressively increasing damping ratios. As aforementioned, the DRM allows for generation of arbitrary 3D seismic wave fields. However, this does not fall in the scope of this preliminary 2D study, which is to illustrate and explain the key mechanisms that govern metamaterial–soil–structure interaction (meta–SSI). Therefore, only vertically propagating shear waves (SH) are considered henceforth.

To generate such vertically propagating wave field and the associated effective forces on the DRM elements of the main model, the following procedure was employed during the first DRM step. Given that the target acceleration time history is at the ground surface of the main model (**Fig. 1**), the motion was de-convoluted first to a depth of 100 m. Then, the vertically propagating wave field was generated, recording the displacement and acceleration time histories of the nodes of interest (i.e., on the DRM elements). Finally, the effective forces P^{eff} were computed and used as input for the main model. Both the de-convolution and the vertical propagation of shear waves are performed using analytical solutions [33,34]. This procedure may sound cumbersome, but it is automated in Real-ESSI, as described by Wang et al. [30]. The user is only required to specify the targeted acceleration and displacement time history at the desired depth (the ground surface in the current study) and the elastic properties of rock and the soil layers.

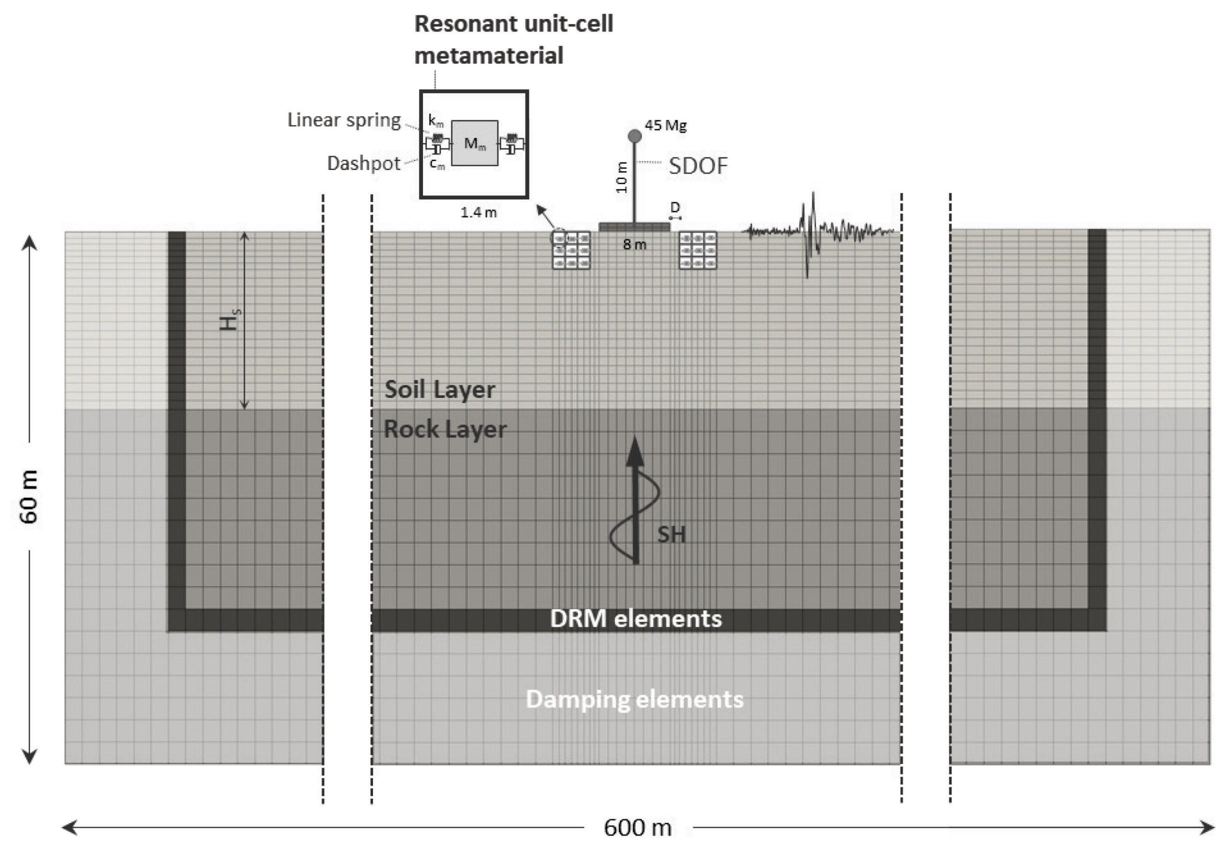

Fig. 1. Overview of a typical 2D DRM FE model with the resonant metamaterials and the SDOF system.

2.2. Soil, Structure and Metamaterial properties

As shown in **Fig. 1**, a uniform elastic/inelastic soil deposit of thickness H_S (variable), shear wave velocity V_S (variable), soil unit weight ρ_s = 1.6 Mg/m^3, Poisson's ratio ν_s = 0.3/0.49 (for the elastic/inelastic case, respectively) and Rayleigh damping ratio of 5% or 2% (elastic or inelastic cases), resting on top of a uniform elastic rock layer ($V_{S,rock}$ = 700 m/s, ρ_{rock} = 2.4 Mg/m^3 and ν_{rock} = 0.3) is considered. Both the soil and the rock layers are modelled with 3D 8-noded brick-type elements (namely, a slice of 3D elements is used for the 2D model). The structure on top of the ground surface is modelled as an idealized SDOF system, 10 m in height, with a rigid foundation of 8 m width (8-node brick elements) and a concentrated mass (45 Mg) on the top node. As depicted in **Fig. 2**, the column of the SDOF system is modelled either using linear elastic beam elements (when the linear elastic response is of interest), or with fiber beam-column elements [35] that exhibit linear elastic-plastic response under flexural loading (when the nonlinear response is of interest). The resulting small-strain (elastic) fundamental natural period of the structure is T_{SDOF} (variable).

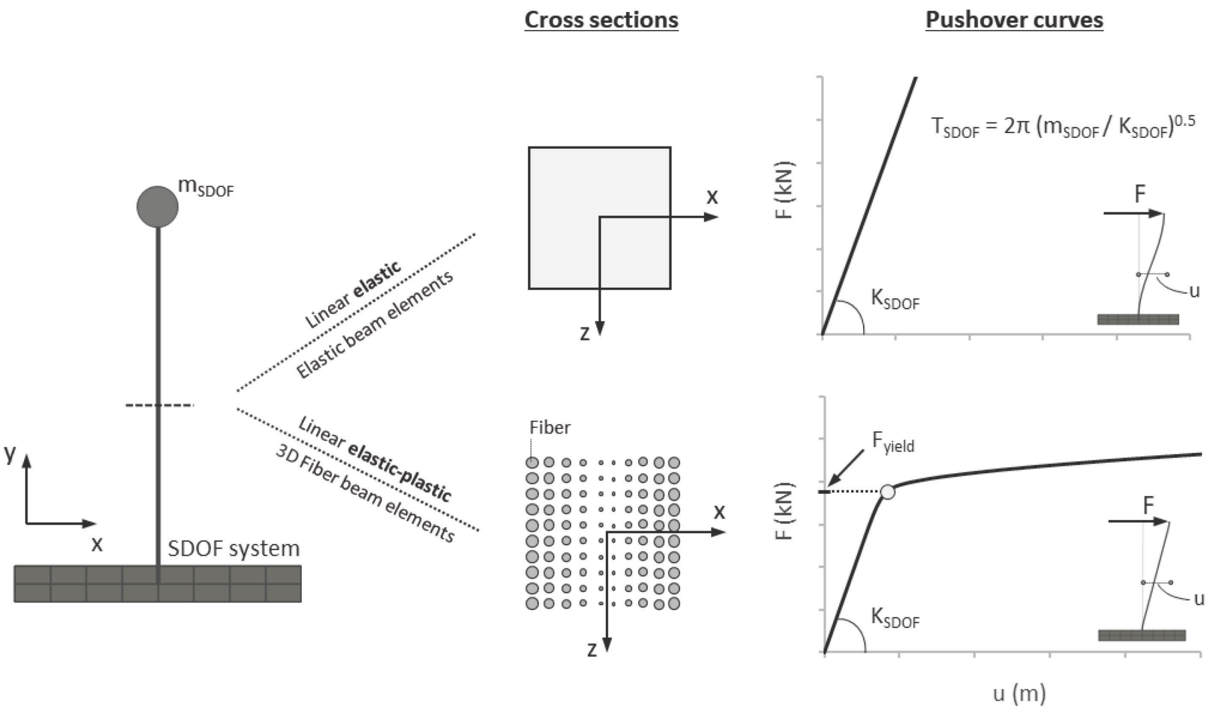

Fig. 2. Elastic and elastoplastic SDOF systems: typical cross sections and resulting monotonic pushover curves.

For the nonlinear SDOF system, the uniaxial nonlinear steel material model initially developed by Menegotto & Pinto [36] and later extended by Filippou et al. [37] is employed, using the calibrated material model parameters of **Table 1**, where σ_y is the yield strength, E_0 the initial elastic modulus, b the strain-hardening ratio (between post-yield tangent and initial elastic modulus), R_0, cR_1, cR_2 are parameters controlling the transition from elastic to plastic regime, and a_1, a_2, a_3, a_4 are isotropic hardening parameters.

Table 1. Input parameters of the uniaxial nonlinear steel material model.

σ_y (kPa)	E_0 (kPa)	b	R_0	cR_1	cR_2	a_1, a_3	a_2, a_4
variable	variable	0.01	100	0.925	0.15	0	55

The resonant metamaterials are organized in two groups of i rows and j columns at the left- and right-hand side of the SDOF structure at distance D from the foundation, embedded into the soil. Each unit cell is a hollow 1.4 m square box, modelled with nearly rigid elastic shell elements, with Young's modulus $E_{unit\ cell}$ = 25'000 GPa, thickness $t_{unit\ cell}$ = 0.2 m, $\rho_{unit\ cell}$ = 2.5 Mg/m^3 and $\nu_{unit\ cell}$ = 0.2. Inside each unit cell there is a concentrated mass M_m (variable), connected to the sides of the box with springs and dashpots. The latter are modelled using Kelvin-Voigt elements of stiffness k_m and viscous damping coefficient c_m. The resulting metamaterial unit cell natural vibration period is equal to T_m (variable). **Table 2** summarizes the main parameters of interest. Their effect on the efficiency of the studied seismic risk mitigation method is evaluated through an extensive parametric analysis. Each parameter is varied within a range of interest, keeping the rest of the parameters constant and equal to their reference value.

Table 2. Reference values for the investigated parameters.

Parameters	Description	Units	Reference Values
T_{SDOF}	Natural period of the SDOF system	sec	0.42
T_m	Natural period of the unit-cell	sec	0.5
M_m	Oscillating mass of the unit-cell	Mg	2.5
ξ_m	Damping ratio of the unit-cell	-	0.06
D	Unit-cells – foundation distance	m	1
$i\,x\,j$	Rows x Columns of the unit-cells	-	3 x 3
V_S	Soil shear wave velocity	m/s	150
H_s	Soil thickness	m	20

2.3 Boundary conditions and interfaces

To meet the plain strain analysis assumptions, the out-of-plane degrees of freedom of all nodes are fixed. This also applies to the top node of the SDOF system, which is free to move horizontally and vertically in plane, resembling the behaviour of a shear building. In this study, the unit cell masses are allowed to oscillate only in the horizontal direction, and fixed boundary conditions are applied at the left, right and bottom side of the model. To avoid any undesired boundary effects, the lateral boundaries of the model are placed far away from the oscillating structures (the model length is 600 m). Although the DRM allows for much smaller computational domains without compromising reliability, since the computational cost for this 2D model is relatively small, a larger model was selected. Finally, all the interfaces of the model (structure-soil, metamaterials-soil) are tied using bonded contact elements.

2.4 Input motions

As summarized in **Table 3**, an artificial Ormsby wavelet [38] (**Fig. 3a**) and 6 real seismic records (**Fig. 4**) (3 pulse-like and 3 non-pulse-like, as categorized by the PEER Ground Motion Database, https://ngawest2.berkeley.edu) are used as seismic excitation at the ground surface, following the aforementioned DRM procedure. The reason for selecting the Ormsby wavelet, is that it can be calibrated to produce a target amplitude spectrum in the frequency domain (by applying the Fast Fourier Transform) with a plateau over a desired frequency range (0.5 to 10 Hz in this case, **Fig. 3b**).

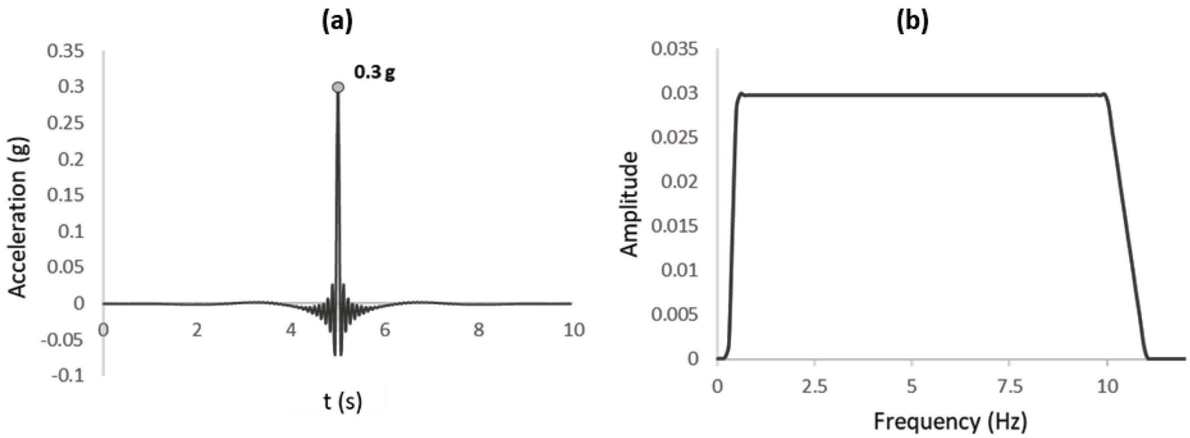

Fig. 3. The Ormsby wavelet: (a) acceleration time history; and (b) frequency amplitude spectrum (Fourier).

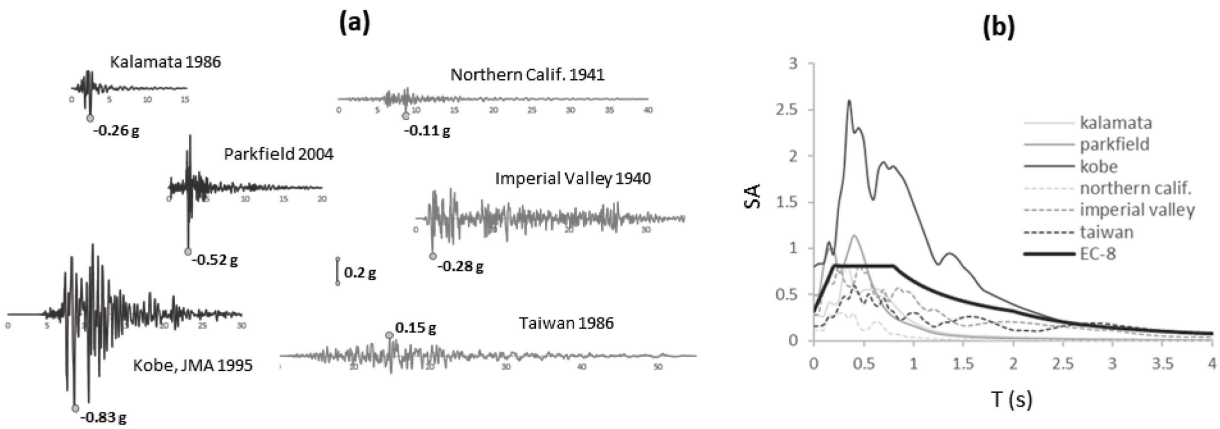

Fig. 4. Ground motions used as seismic excitation at the ground surface: (a) pulse-like (left) and non-pulse-like (right) seismic records; along with (b) their pseudo-acceleration response spectra (SA). The EC-8 [39] elastic response spectrum (PGA = 0.24g, Ground Type B, Importance Class II) is given for reference.

Table 3. Utilized earthquake ground motion records as categorized by the PEER Ground Motion Database

Event	Year	Station	Mag.	Direction	type
Kalamata, Greece	1986	Kalamata (bsmt)	5.4	H2	Pulse-like
Parkfield-02, California	2004	Cholame 3E	6	H1	Pulse-like
Kobe, Japan	1995	KJMA	6.9	H1	Pulse-like
Northern California-01	1941	Ferndale City Hall	6.4	H1	No Pulse-like
Imperial Valley-02	1940	El Centro Array #9	6.95	H1	No Pulse-like
Taiwan SMART1 (45)	1986	SMART1 C00	7.3	H2	No Pulse-like

3. The principal seismic response reduction mechanism

In order to understand and explain the basic working principle of the studied resonant metamaterials for seismic risk reduction, a simplified case is analyzed in this section. To evaluate the effect of the resonant metamaterials on free-field soil response, the base of the soil layer (V_S = 150 m/s) is excited by horizontal sinusoidal motions in the absence of the SDOF system. **Figure 5** compares the maximum accelerations a_{max} on the ground surface (point A) for steady-state response, with (T_m = 0.45, 0.55 and 0.65 s) and without metamaterials, for different input motion periods (T_{inp} = 0.1 – 1 s). A significant reduction in the response can be observed when T_{inp} is close to T_m (denoted by the vertical lines in **Fig. 5**).

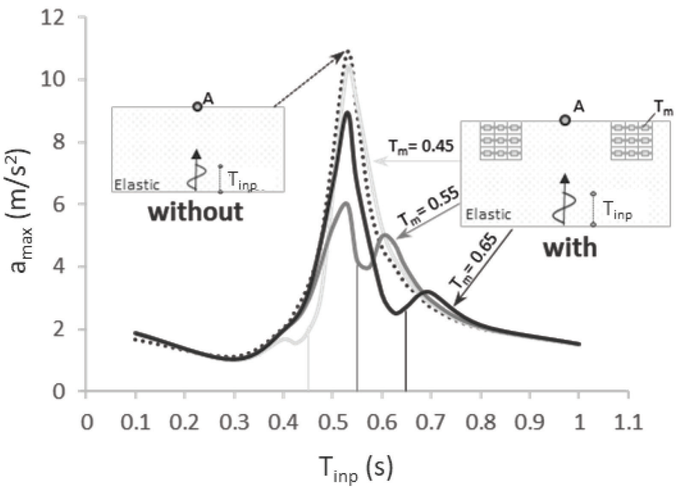

Fig. 5. The effect of resonant metamaterials on free-field response: maximum accelerations a_{max} at point A, with (T_m = 0.45, 0.55 and 0.65 s) and without resonant metamaterials, in function of T_{inp}.

Indeed, if we normalize T_{inp} with T_m and the maximum acceleration a_{max} with $a_{0,max}$ (the maximum acceleration without metamaterials), it becomes evident that the maximum reduction ($a_{max}/a_{0,max} < 1$) is achieved when $T_{inp}/T_m \rightarrow 1$ but is less than 1, while for values greater than 1 a small—yet non-negligible—amplification takes place (**Fig. 6a**). These trends can be easily interpreted by looking at the phase difference Φ between point A on the ground surface and point B of an oscillating unit cell mass (**Fig. 6b**). For $T_{inp}/T_m = 1$, where the resonant metamaterials are oscillating at their natural period, and therefore with maximum amplitude, they also happen to oscillate with phase difference $\Phi = \pi/2$ with respect to the surrounding soil. Exactly because of such out-of-phase oscillation, the resonant metamaterials are capable of exerting forces in the opposite direction compared to the movement of the surrounding soil, thus decreasing its acceleration.

Ideally, the maximum reduction could have been achieved for $\Phi = \pi$, where the oscillating masses are always moving in the opposite direction compared to the soil. But as Φ moves from π/2 to π, the metamaterial mass oscillation amplitude reduces as well, making them less efficient. In the same way, for $0 < \Phi < \pi/2$, where the metamaterial masses are oscillating in-phase with the surrounding soil, the response of the latter can be amplified. However, since the metamaterial masses are oscillating at periods different from their natural period T_m, their oscillation amplitudes are reduced. As a result, the observed free-field response amplification is less pronounced than the beneficial free-field response reduction they can offer. The reason why the three curves of **Fig. 6a**. are not identical lies in the dynamic characteristics of the soil. Specifically, for T_m = 0.55 s, the larger reduction that appears at $T_{inp}/T_m = 1$ compared to the other two cases can be attributed to the fact that the soil also oscillates very close to its natural period (T_s = 0.53 s), subjecting the resonant metamaterials to larger input excitation, which results in larger oscillation amplitudes of their masses.

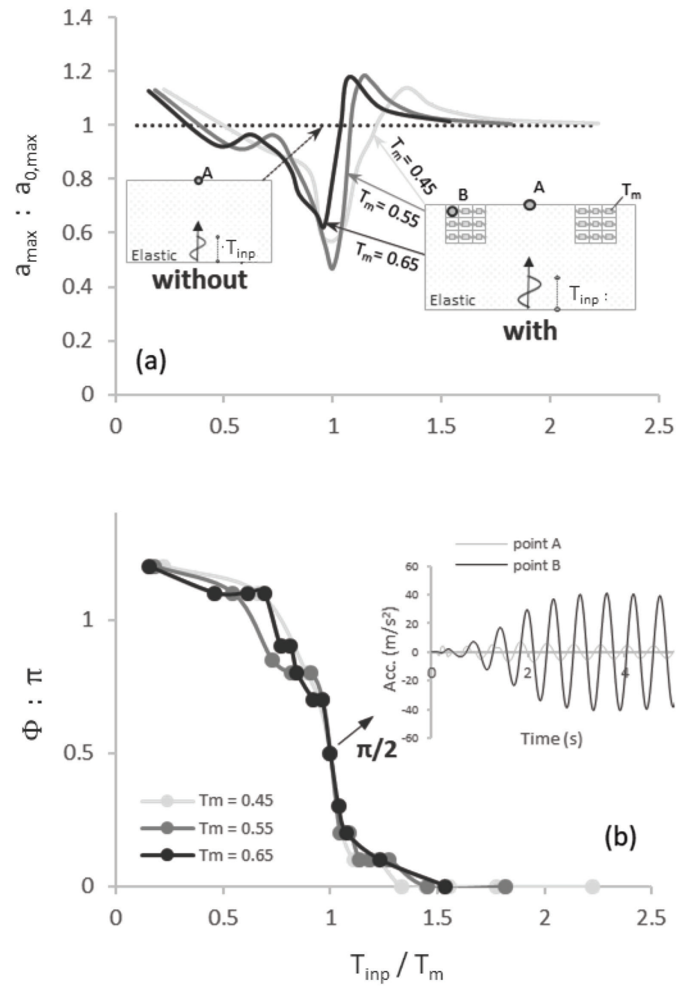

Fig. 6. The effect of resonant metamaterials on free-field response: (a) normalized maximum accelerations $a_{max}/a_{0,max}$ at point A for T_m = 0.45, 0.55 and 0.65 s, in function of T_{inp}/T_m; and (b) phase difference Φ between point A on the ground surface and point B on an oscillating unit cell mass for T_m = 0.45, 0.55 and 0.65 s, in function of T_{inp}/T_m. The inset shows the acceleration time histories of points A and B for T_m = 0.55 s.

Finally, it is worth noting that the case of empty boxes (i.e., complete absence of vibrating metamaterial masses) and the case of very stiff springs (i.e., masses fixed to the outer box) gave practically the same results as the free-field case (no metamaterials), verifying that the resonant mechanism described above is the one responsible for the observed behaviour under linear-elastic soil conditions. However, as it will be shown later on, this is not the case under nonlinear soil response.

4. Elastic structure on elastic soil

Starting with the linear-elastic conditions, both for the soil and the structure (SDOF system), **Fig. 7** compares the acceleration and relative displacement time histories of the structure, excited by the Ormsby wavelet ("applied" at the ground surface using the DRM), with and without resonant metamaterials. The reference parameters of **Table 2** are used, except for T_m = 0.45 s (deliberately chosen to be a bit larger than $T_{SDOF,ref}$ = 0.42 s, so that the resonating masses will be oscillating out-of-phase with the soil, achieving the desired reduction of the excitation that reaches the SDOF system). The resonant metamaterials can be seen to marginally reduce the first excitation cycles (as they need a few excitation cycles to start oscillating), thereafter increasing their efficiency.

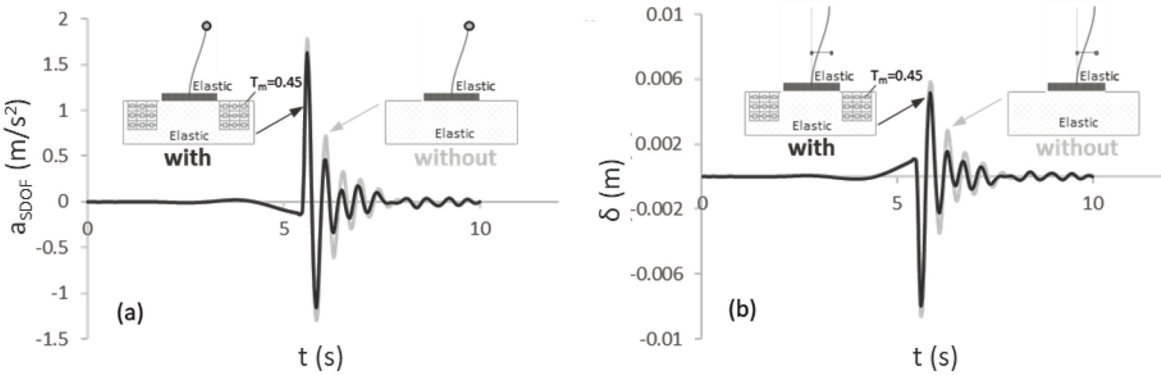

Fig. 7. Elastic structure on elastic soil (**Table 2** reference parameters, except for T_m = 0.45 s) subjected to the Ormsby wavelet. Time histories of: (a) acceleration a_{SDOF} ; and (b) drift δ (relative horizontal displacement) of the SDOF system with and without resonant metamaterials.

In order to conduct a detailed parametric analysis and present the results in the most concise way, there is a need for a single engineering demand parameter that can reflect most of the information entailed in the time histories of response. The maximum acceleration or the maximum drift of the SDOF system cannot reveal the beneficial role of resonant metamaterials for the entire time history analysis. A candidate engineering demand parameter may be found in an energy-based approach, which has lately been used for seismic design of soil-structure systems [40–42]. Such an informative energy-based damage index is the plastic energy dissipation accumulated during seismic loading in the SDOF system [41], which better reflects the overall damage of the structure (not only its peak response). The plastic energy dissipation should not be confused with the plastic work (or hysteretic energy). As pointed out by Yang et al. [42], the plastic work is the sum of plastic energy dissipation (irrecoverable), which is defined as the amount of heat (and other forms of energy) transformed from mechanical energy during an irreversible dissipative process, and plastic free energy (conditionally recoverable), which can be developed due to particle rearrangements inside the inelastic material and may even reach 40% of the total plastic work. Thus, for the inelastic SDOF system studied herein, the accumulated plastic energy dissipation is selected as the engineering demand parameter to evaluate the efficiency of resonant metamaterials. On the other hand, for the elastic SDOF system, all the incoming seismic energy that is transformed to kinetic and strain energy alternatingly during its oscillation, will be totally recovered in the end. This means that no accumulation of energy (as for the inelastic SDOF system described earlier) can be extracted at the end of the analysis. To overcome this shortcoming, an ad-hoc solution is adopted for the elastic SDOF system. The strain energy developed in the elastic beam elements of the SDOF system may serve as a good indicator of the potential damage that would have happened if it was inelastic.

Figure 8 presents the accumulated strain energy time histories at the base of the SDOF system, with and without metamaterials. As expected, the accumulated strain energy becomes zero at the end of the analysis. However, the area below each accumulated strain energy time history curve could be a good indicator of the potential structural damage of the SDOF system. In other words, the larger the area below the accumulated strain energy curve, the more damage is expected for an inelastic structure. In this way, normalizing the area corresponding to the case with metamaterials by the area corresponding to the case without (unprotected structure), a direct comparison can be made. The smaller than 1 this ratio, the more effective the resonant metamaterial are. Conversely, normalized accumulated strain energy ratio greater than 1 indicates that the SDOF system experiences amplification in its response due to the presence of resonant metamaterials. For example, in **Fig. 8**, the value 0.74 would correspond to 26% reduction in the accumulated strain energy throughout the entire time history because of resonant metamaterials' impact. Henceforth, for the linear elastic parametric analyses, the aforementioned ratio is used and called Equivalent Strain Energy Ratio ($ESER$).

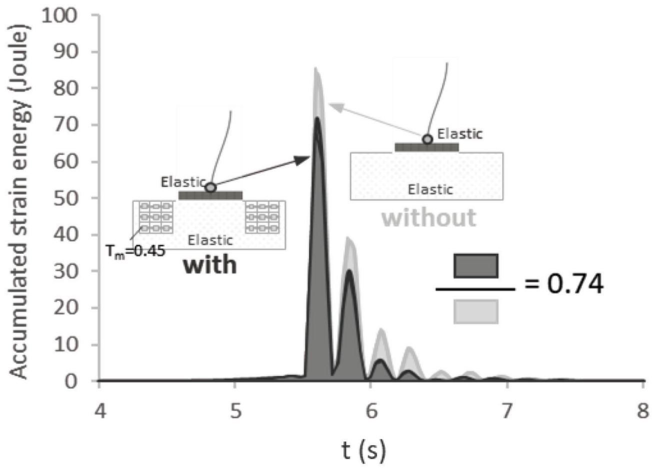

Fig. 8. Elastic structure on elastic soil (**Table 2** reference parameters, except for T_m = 0.45 s) subjected to the Ormsby wavelet. Comparison of accumulated strain energy time histories at the base of the SDOF system, with and without resonant metamaterials. The area below each accumulated strain energy time history may serve as an indicator of potential structural damage.

Figure 9 summarizes the main results obtained from the linear elastic parametric analysis. The parameter of interest is always plotted on the horizontal axis, while the vertical axis plots the previously defined $ESER$ (notice that the thick horizontal line at $ESER$ = 1, is the result of normalizing the "without" case by itself). For the first—and probably most important—parameter of interest, the natural period of the resonant metamaterials (T_m), it is immediately observed that the maximum reduction of $ESER$ occurs for T_m = 0.45 s (slightly higher than $T_{SDOF,ref}$ = 0.42 s). The main reason is the out-of-phase oscillation of the unit cell masses relative to the oscillation of the surrounding soil, at excitation periods close to the resonant period of the structure. Such resonance becomes more pronounced for larger oscillation amplitudes of the unit cell masses. For this to occur, an earthquake excitation with frequency content able to amplify the resonant period of the metamaterials is needed. For example, the pseudo-acceleration response spectrum of the 1940 Imperial Valley earthquake, which gives the largest reduction at T_m = 0.45 s (**Fig. 9**), exhibits a peak SA close to T = 0.45 s (**Fig. 4b**). On the contrary, the 1941 N. California earthquake, which gives results that deviate visibly from the trend of all other excitations, exhibits a trough close to T = 0.45 s (**Fig. 4b**). Interestingly, the maximum $ESER$ reduction for the 1941 N. California earthquake is for T_m = 0.7 s, which is not that close to $T_{SDOF,ref}$, and can be clearly associated to the SA close to 0.7 s (**Fig. 4b**), which seems to force the metamaterial unit cell masses to oscillate at this period. Given the inconsistency of the 1941 N. California earthquake seismic motion compared to all other excitations, its results are plotted with high transparency to make the figures more readable.

Keeping T_m constant and equal to its reference value of 0.5 s, while varying the natural period of the SDOF system (T_{SDOF}), it can again be noticed that the maximum reduction of $ESER$ takes place for $T_{SDOF} < 0.5$ s (= $T_{m,ref}$), inside the "out-of-phase" area of **Fig. 9**. It is worth noting that the amplification takes place for $T_{SDOF} > 0.5$ s, inside the "in-phase" area, where the metamaterial masses are mostly moving in-phase with the soil. This undesirable amplification effect is smaller compared to the maximum reduction that can be achieved (since the metamaterial masses are not oscillating at their natural period), and can be avoided with proper tuning of the natural period of the resonant metamaterials (i.e., T_m should be equal or a bit larger than T_{SDOF} for elastic systems).

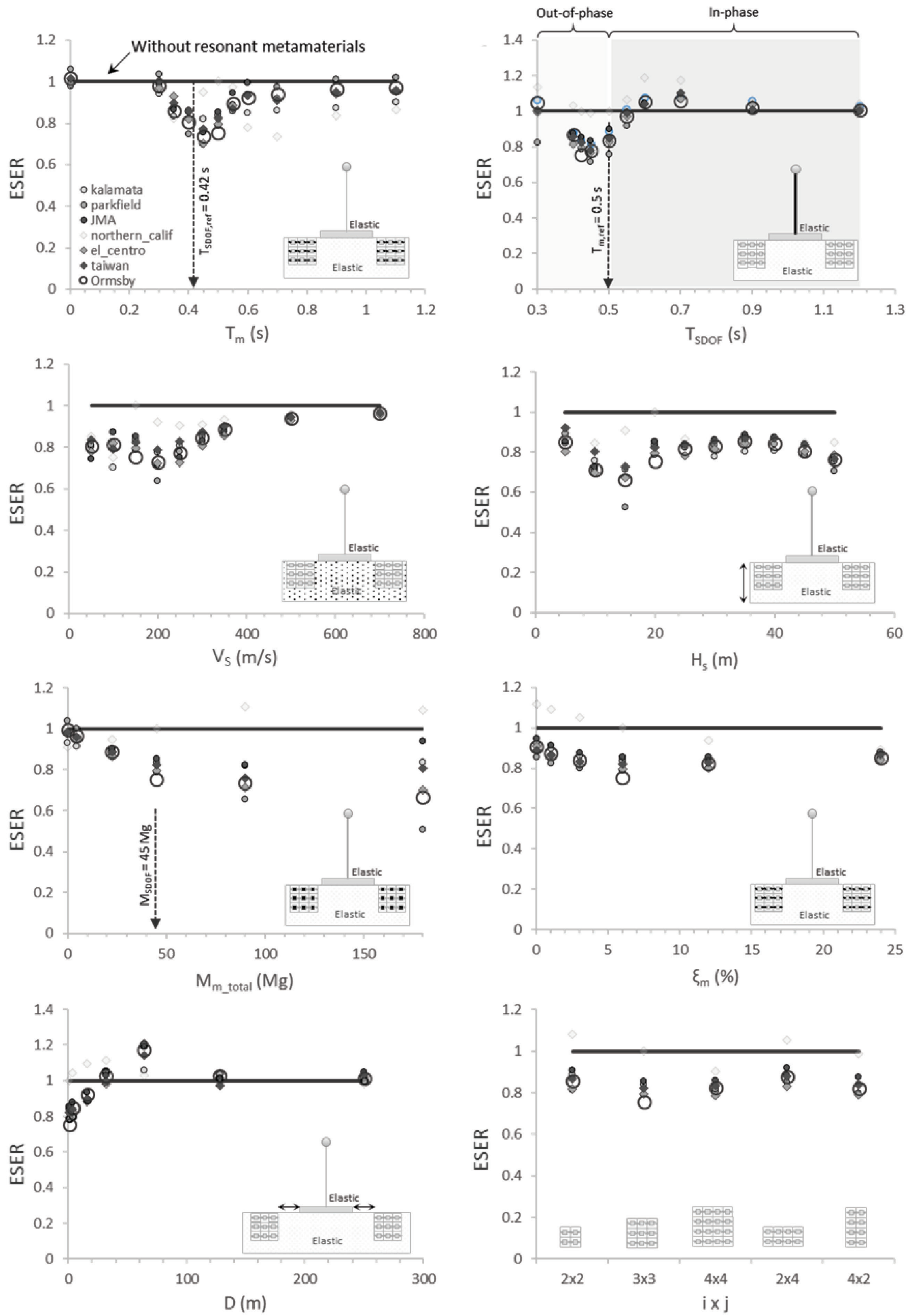

Fig. 9. Elastic structure on elastic soil parametric analysis: effect of each investigated parameter on $ESER$. $ESER$ < 1 corresponds to a beneficial effect of the metamaterials, while $ESER$ > 1 to detrimental effect.

The total oscillating mass of the resonant metamaterials $M_{m,total}$ is also affecting the response significantly. As shown in **Fig. 9**, the reduction of $ESER$ grows with the increase of $M_{m,total}$, at least up to reasonable values (close to the total mass of the SDOF system). For $M_{m,total}$ larger than the SDOF mass, the dynamic behaviour of the entire system changes radically; this scenario was deemed unrealistic to be investigated further. For zero mass (i.e., empty unit cells), the almost negligible reduction of $ESER$ is attributed to the kinematic interaction between the empty boxes and the incoming seismic waves, the so-called "shadow" effect. This additional reduction mechanism becomes more pronounced as the seismic wavelength approaches the metamaterials embedment depth (reminiscent of [2–4]). As will be shown later for the inelastic soil conditions, as the seismic wavelengths become shorter (approaching the metamaterials size), such kinematic interaction effect becomes more pronounced.

The damping ratio ξ_m of the resonant metamaterials is investigated next. From the results of **Fig. 9**, an optimal $\xi_m \approx 6$ % can be deduced. Higher damping reduces the oscillation amplitude of the internal metamaterial masses, reducing their effectiveness as they move out-of-phase with the surrounding soil, while very small ξ_m leads to very high amplitude (theoretically infinite) oscillations of the unit cell masses, also leading to a reduction of their efficiency.

Another key parameter is the distance D of the resonant metamaterials from the structure. As expected, the maximum reduction is achieved when the metamaterials are right next to the structure. Somewhat surprising, however, is the amplification of $ESER$ for large D. This is attributed to the waves that are generated by the vibration of the internal masses: propagating through the soil, they are reflected at the soil-bedrock interface, eventually exciting the SDOF system and amplifying its response. As it will be shown later on, this adverse effect fades out when soil inelasticity is accounted for.

The last metamaterial parameter explored herein is the geometric configuration of the resonant metamaterial unit cells, i.e., the number of rows and columns, i and j, of the unit cells, respectively. Keeping the total unit cell mass constant (as well as the rest of the parameters), **Fig. 9** indicates that the deeper into the soil the resonant metamaterials are embedded, the more efficient they become (the 3x3 configuration achieves better performance than the 2x2; the 4x4 is better than the 3x3, with a few discrepancies; and 4x2 is better than 2x4). This effect becomes more pronounced when inelastic soil response is considered, and is attributed to the kinematic interaction between the metamaterials and the vertically propagating shear waves ("shadow" effect).

Another crucial parameter that defines the efficiency of resonant metamaterials in mitigating the seismic risk is the shear wave velocity V_S of the soil (soil stiffness). **Figure 9** shows that the resonant metamaterials become more effective for softer soils. Conversely, the increase of V_S leads to a reduction of the efficiency of the resonant metamaterials (for $V_S \geq 500$ m/s, $ESER \rightarrow 1$): soil compliance is needed to accommodate the forces exerted by the metamaterials. The maximum ESER reduction that is observed for $V_S = 200$ m/s is associated with the natural period of the soil layer (close to 0.5 s), which happens to coincide with the period of the resonant metamaterials. Such double resonance is beneficial, as it provides increased energy to the metamaterials, increasing the oscillation amplitudes of the unit cell masses, consequently leading to larger reduction of system response, as revealed by $ESER$.

The last investigated parameter is the soil thickness H_S. The maximum reduction of $ESER$ is observed for H_S = 15 m, and is most probably related to the seismic waves reflected at the soil-bedrock interface, which return and excite the SDOF system with opposite phase, to further reduce its response. This effect is directly related to the assumption of rigid bedrock. In the case of half-space or compliant base conditions, the waves will be fully or partially refracted, potentially reducing the observed effect.

Finally, it is worth mentioning that the majority of the earthquake records used in the analyses follow similar trends in all of the presented diagrams of **Fig. 9**. Quite remarkably, the Ormsby wavelet follows these trends, rendering it a promising candidate for representing real seismic records with a single artificial motion.

5. Nonlinear structure on elastic soil

Elastic analysis is useful to identify key mechanisms and trends governing the behaviour of the studied resonant metamaterial–soil–structure system. However, during strong seismic events, both the structure and the soil will exhibit nonlinear response. In this section, the impact of structural inelasticity is evaluated, while the soil remains elastic. The nonlinear response of the structure is expected to elongate its effective natural period, reducing (if not completely cancelling) the effectiveness of the resonant metamaterials, which will be vibrating in-phase with the soil at the elongated period of the SDOF system.

As described earlier (**Fig. 2**), the inelastic SDOF system is assumed linear-elastic–plastic. To produce the desired yield force F_{yield}, the uniaxial nonlinear steel material model of the fiber beam-column elements is calibrated accordingly (**Table 1**). In the same figure, notice that the area of the fibers in the cross section of the fiber beam element is progressively increasing away from its neutral axis, so that all fibers yield simultaneously. F_{yield} is calculated by multiplying the mass of the SDOF system with the design acceleration from EC8 [39], assuming a design/inelastic spectrum for PGA = 0.24 g, ground type that varies depending on V_S and H_s, and Importance Class II. The same ground motions as in the elastic case are used, with a few modifications: 4 separate Ormsby wavelets are applied with increasing amplitudes (x2 to x5) to progressively drive the SDOF system into its inelastic regime, while the 1941 N. California and the 1986 Taiwan records are multiplied by 2.5 and 2.0 respectively, to ensure that the structure will always enter its inelastic regime. As mentioned earlier, the most appropriate damage index to present the results for the inelastic SDOF system is the accumulated plastic energy dissipation. Henceforth, the parametric results are presented in function of the Accumulated Plastic Energy Dissipation Ratio ($APEDR$), which is defined as the plastic energy dissipation accumulated in the bottom element of the SDOF system throughout the entire time history analysis of the "with" case, normalized by the respective "without" case. The latter is normalized by itself, resulting to a horizontal straight line at $APEDR = 1$.

Before starting with the parametric analyses, the role of the SDOF system behaviour factor q is briefly explored in **Fig. 10** (the remaining parameters are equal to their reference values, **Table 2**). It is observed that the increase of q (i.e., the increase of structural inelasticity) leads to a pronounced increase of $APEDR$. For $q \geq 4$, the presence of resonant metamaterials leads to amplification of response ($APEDR > 1$). This confirms the previously discussed concern about the elongation of the SDOF effective period. However, proper tuning of the resonant metamaterials at longer periods, accounting for the expected period elongation of the structure, could partially overcome this shortcoming.

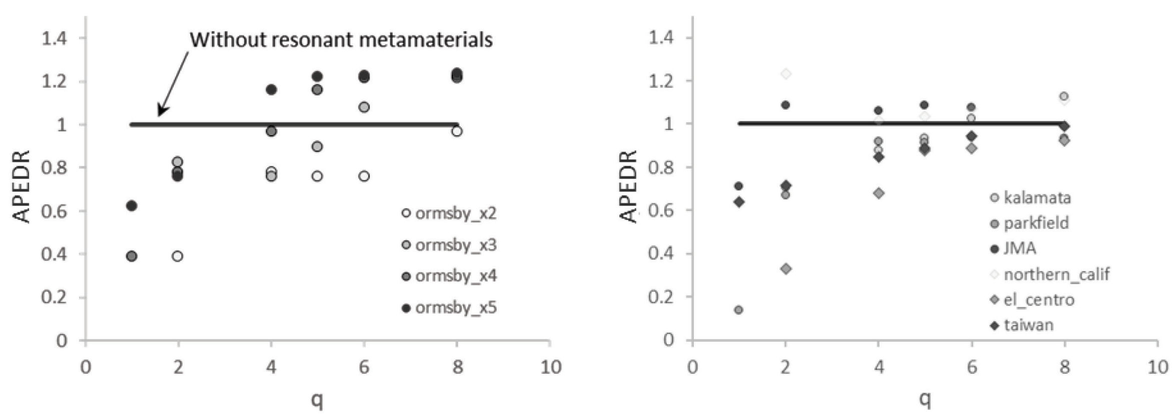

Fig. 10. Nonlinear structure on elastic soil subjected to scaled up Ormsby wavelets (left) and real records (right). The effect of structural inelasticity, expressed through the behavior factor q, on the Accumulated Plastic Energy Dissipation Ratio ($APEDR$). The effect of metamaterials is beneficial when $APEDR < 1$.

This is confirmed in **Fig. 11**, which summarizes the results of the parametric analysis for q = 4. Specifically, in the first two plots (top) which examine the effect of T_m, the presence of resonant metamaterials is always beneficial for $T_m \geq 0.7$ s. A similar conclusion can be drawn by looking at the next two diagrams, where the effect of T_{SDOF} is explored; for $T_{m,ref}$ = 0.5 s, the response of the SDOF system is reduced when $T_{SDOF} < 0.2$ s (with the exception of the 1995 Kobe JMA record). The next two plots explore the influence of the total vibrating mass $M_{m,tot}$ ($T_{m,ref}$ remains equal to 0.5 s, and is not properly tuned on purpose, to expose unintended amplification effects). Depending on the amplitude of the excitation or, equivalently, how deeply into its inelastic regime the SDOF system is driven, metamaterials can play a beneficial (when vibrating out-of-phase with the soil at periods close to the elongated effective period of the SDOF system) or a detrimental role (when they vibrate in-phase). The last investigated parameter is V_S, which gives similar results to the elastic case, but with a more significant drop of $APEDR$ with the decrease of soil stiffness.

The effect of the remaining parameters is not presented herein, as the most notable trends are similar to the previously discussed elastic case. It is worth noting, that the Ormsby wavelets with gradually increasing amplitudes could reproduce the results of the real seismic records quite successfully.

6. Nonlinear structure on nonlinear soil

Despite the computation attractiveness of elastic modelling, in reality soil exhibits nonlinear response even at small strains. During strong earthquakes, inelastic soil response is inevitable and can affect dynamic SSI to a great extent [43–45]. It is therefore crucial to evaluate its influence on the protective role of resonant metamaterials. To that end, a von Mises elastoplastic constitutive model with Armstrong-Frederick nonlinear kinematic hardening [46] and associated flow rule is employed. This model is a fairly simple yet effective constitutive model for pressure independent materials (such as saturated clay) [47]. The parameters of the constitutive model for the reference case are summarized in **Table 4**, where ρ is the unit weight, E is the elastic modulus, ν is the Poisson's ratio, R is the Von Mises radius (which controls the size of the elastic region), and h_a and c_r are two parameters that control the post-yield hardening [38], calibrated to realize the desired undrained shear strength S_u of the soil. Specifically, h_a is the post-yield initial stiffness, while the h_a / c_r ratio defines the plateau of the back stress saturation.
The shear modulus to undrained shear strength ratio G_0/S_u is selected to be equal to 1000. Thus, for the reference case, where V_S = 150 m/s, the corresponding $S_u = 36$ kPa (ground type E, according to EC8 [39]). As shown in **Fig. 12**, the resulting normalized secant shear modulus – shear strain curve ($G/G_0 - \gamma$) is in reasonably good agreement with the experimental curves of Vucetic & Dobry [48] for PI = 30 (where PI is the plasticity index of the soil). On top of the energy dissipation due to soil inelasticity (plastic energy dissipation), a Rayleigh damping ratio of 2% (viscous energy dissipation) is used to account for the energy dissipation in soil due to the viscous coupling between soil grains and pore fluids [47,49].

Table 4. Input parameters of the von Mises elastoplastic model with Armstrong-Frederick nonlinear kinematic hardening for the reference case.

ρ (Mg/m^3)	E (MPa)	ν (-)	R (kPa)	h_a (MPa)	c_r (-)
1.6	107.28	0.49	2.8	250	4200

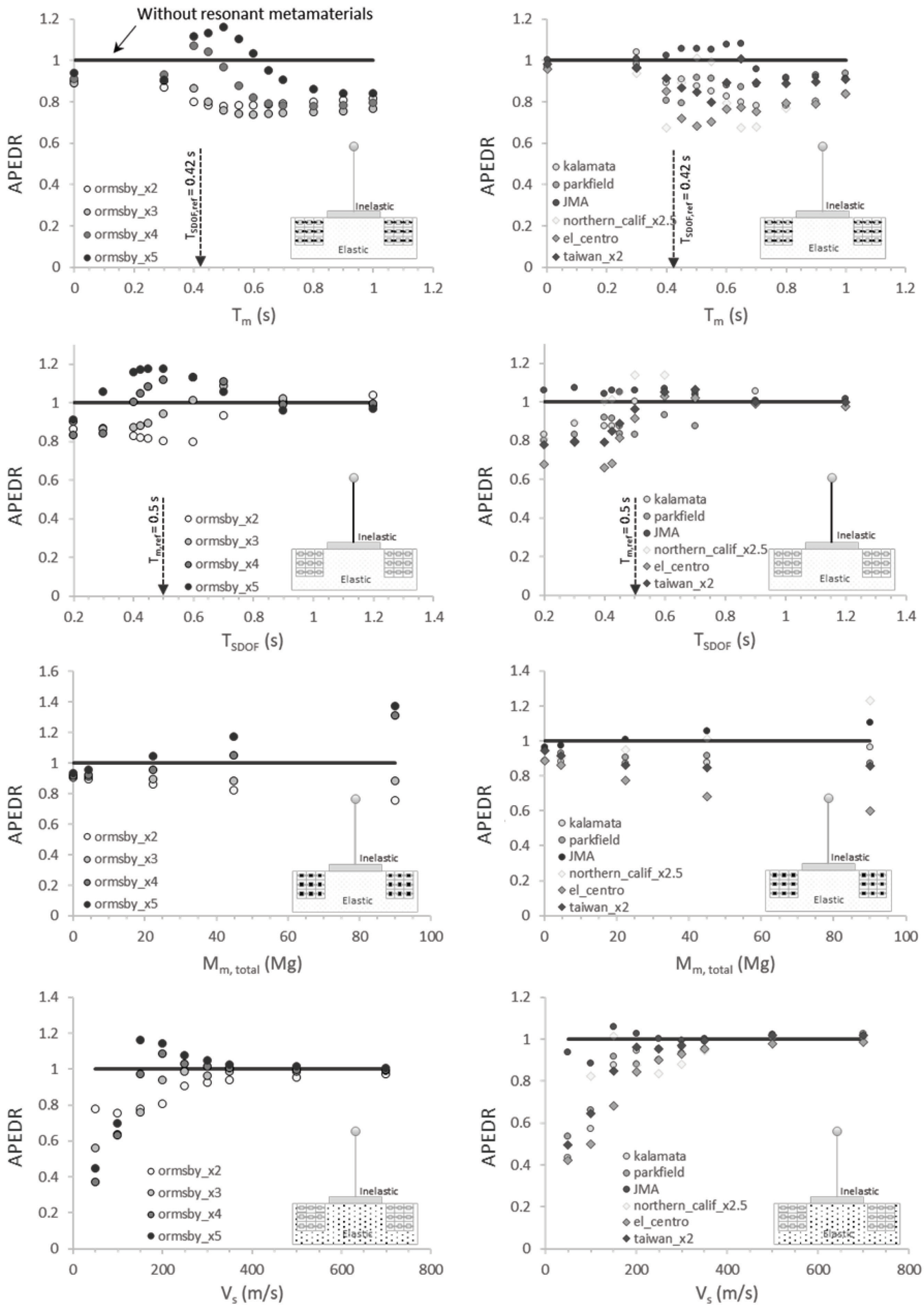

Fig. 11. Nonlinear structure on elastic soil parametric analysis: effect of each investigated parameter on $APEDR$. $APEDR$ < 1 corresponds to a beneficial effect of the metamaterials, while $APEDR$ > 1 to a detrimental effect.

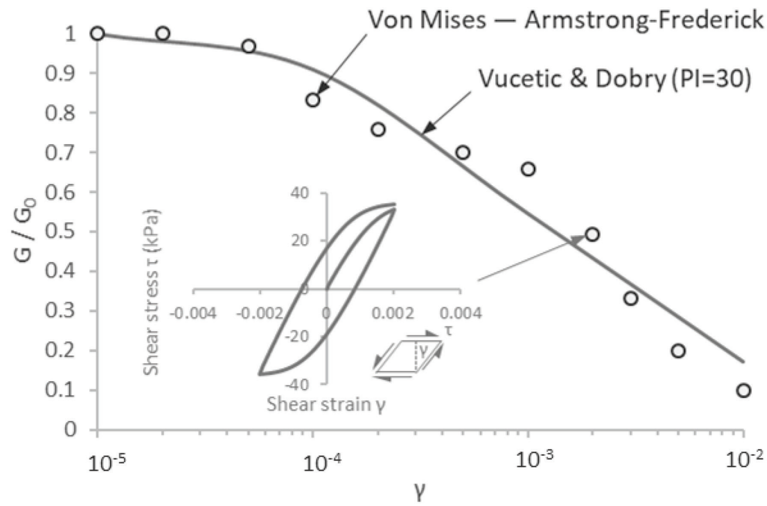

Fig. 12. Nonlinear soil response modelled with a von Mises–Armstrong-Frederick soil model, for G_0 / S_u= 1000 (S_u= 36 kPa for the reference case): comparison of computed $G/G_0 - \gamma$ degradation curves to the experimental curves of Vucetic & Dobry (1991). The inset plots the shear stress-strain $(\tau - \gamma)$ response for γ = 0.002.

As previously, 4 Ormsby wavelets of gradually increasing amplitude and 6 real seismic records are used in the parametric analysis. Detailed time history results are initially presented to gain insights on system response. **Figure 13** compares the drift δ (relative displacement) time history and the base shear–drift $(F - \delta)$ response of the protected ("with") and the unprotected ("without") inelastic SDOF systems, excited by the 1986 Kalamata record. The presence of the resonant metamaterials leads to a small reduction of the maximum and residual drift δ (**Fig. 13a**). Their beneficial effect is revealed in **Fig. 13b**, where a quite significant drop in ductility demand can be observed. **Figure 14a** plots the incremental plastic energy dissipation time history of the bottom column elements for the two studied cases. Although the first peak is barely reduced, a significant reduction of the following ones is observed. By simply summing up the values of this diagram, the accumulated plastic energy dissipation in the bottom elements can be derived (**Fig. 14b**). The latter will be used again to present the parametric analysis results, as the most representative energy-based damage index. Quite remarkably, for this specific example, the resonant metamaterials were able to reduce the accumulated plastic dissipation by almost 50%.

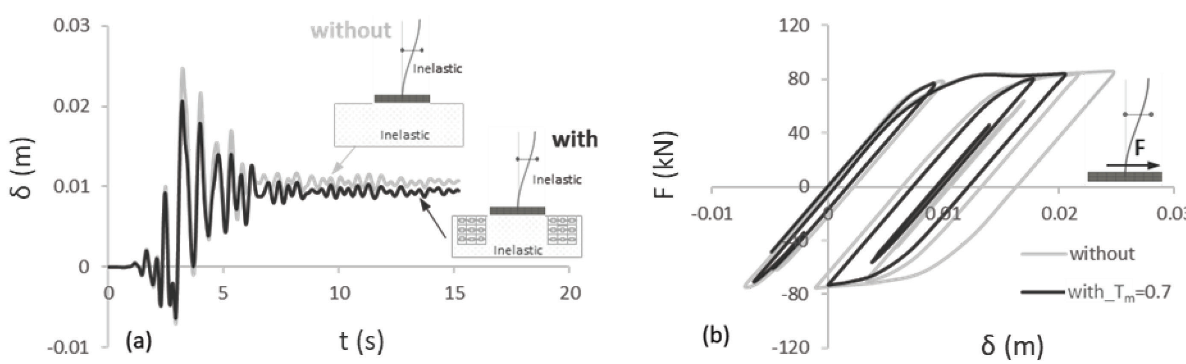

Fig. 13. Nonlinear structure on nonlinear soil (all parameters are equal to their reference values of **Table 2**, except for T_m = 0.7 s). Comparison of protected with metamaterials ("with") to unprotected ("without") SDOF system subjected to the 1986 Kalamata record: (a) drift δ time histories; and (b) base shear–drift $(F - \delta)$ response.

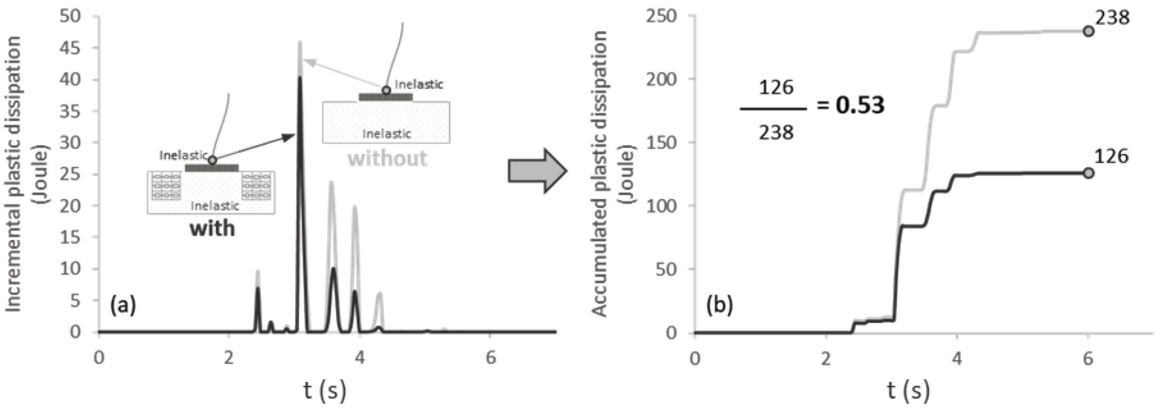

Fig. 14. Nonlinear structure on nonlinear soil (all parameters are equal to their reference values of **Table 2**, except for T_m = 0.7 s). Comparison of protected with metamaterials ("with") to unprotected ("without") SDOF system subjected to the 1986 Kalamata record: (a) incremental plastic energy dissipation; and (b) accumulated plastic energy dissipation of the SDOF system's bottom element.

The parametric analysis results are summarized in **Figs. 15a,b**. Starting with the crucial parameter T_m, two main areas of significant reduction of $APEDR$ are noticed in **Fig. 15a**; the first one is close to T_m = 0.4 s and the second one close to T_m = 0.7 s, with most of the motions being more biased to one of these values (either 0.4 or 0.7). For example, significant $APEDR$ reduction that occurs at T_m = 0.45 s is observed for the 2004 Parkfield earthquake record, while a similar reduction at T_m = 0.7 s is observed for the 1986 Taiwan earthquake record. This can be explained by looking at the Fourier spectra of the SDOF system top node acceleration for the 2004 Parkfield and the 1986 Taiwan excitations in **Figs. 16** and **17**, respectively. **Figure 16a** compares the amplitudes of the elastic and the inelastic analysis of the reference unprotected SDOF ("without") for the 2004 Parkfield earthquake. As expected, the elastic SDOF system exhibits its main response peak close to 2.4 Hz (corresponding to $T_{SDOF,ref}$ = 0.42 s), while the inelastic one has two peaks; one at 2.4 Hz and another one close to 1.6 Hz (notice that the elastic analysis has a smaller peak at 1.6 Hz too, which stands for the resonant frequency of the combined SDOF system and soil model). For the inelastic analysis, the peak at 1.6 Hz is due to the elongation of the period of the inelastic SDOF system as it yields and, also, coincides with the elastic resonant frequency of the combined model.

So, in order to protect the inelastic SDOF system, one would wonder which one of those two peaks is more important to target for reduction: the peak at 1.6 Hz (corresponding to 0.625 s, for which T_m should be 0.7 s, **Fig. 16b**), or the peak close to 2.4 Hz (corresponding to 0.42 s, for which T_m should be 0.45 s, **Fig. 16b**)? We already know the answer for this specific example, since for the 2004 Parkfield excitation, T_m = 0.45 s leads to greater reduction in plastic dissipation ratio than T_m = 0.7 s (**Fig. 15a**), and this is mainly attributed to the fact that the SDOF system is not driven deeply into its inelastic regime (apart from the first big pulse, it remains almost elastic afterwards, as shown in **Fig. 18a**). Thus, targeting the elastic period of the SDOF system with T_m = 0.45 s results in larger reduction of the plastic dissipation ratio. On the contrary, for the 1986 Taiwan earthquake, where T_m = 0.7 s is the optimum value (**Fig. 15a**), the Fourier spectrum of the reference unprotected SDOF system has a significant peak close to 1.5 Hz (corresponding to 0.67 s, for which T_m = 0.7 s could reduce the amplitude, **Fig. 17b**). This is close to the elongated effective period of the inelastic SDOF system and, again, coincides with the elastic resonant frequency of the combined model. Indeed, **Fig. 18b** shows that the SDOF system is highly inelastic when subjected to the 1986 Taiwan excitation. Since we are mainly interested in reducing the plastic energy dissipation of highly inelastic SDOF systems (and not of nearly elastic ones), T_m = 0.7 s is used as a reference value for the remaining parametric analyses. Its efficacy is clearly demonstrated in **Fig. 15a**, in the relevant T_{SDOF} plots, where the maximum reduction of $APEDR$ occurs close to $T_{SDOF,ref}$ = 0.42 s, which was the target.

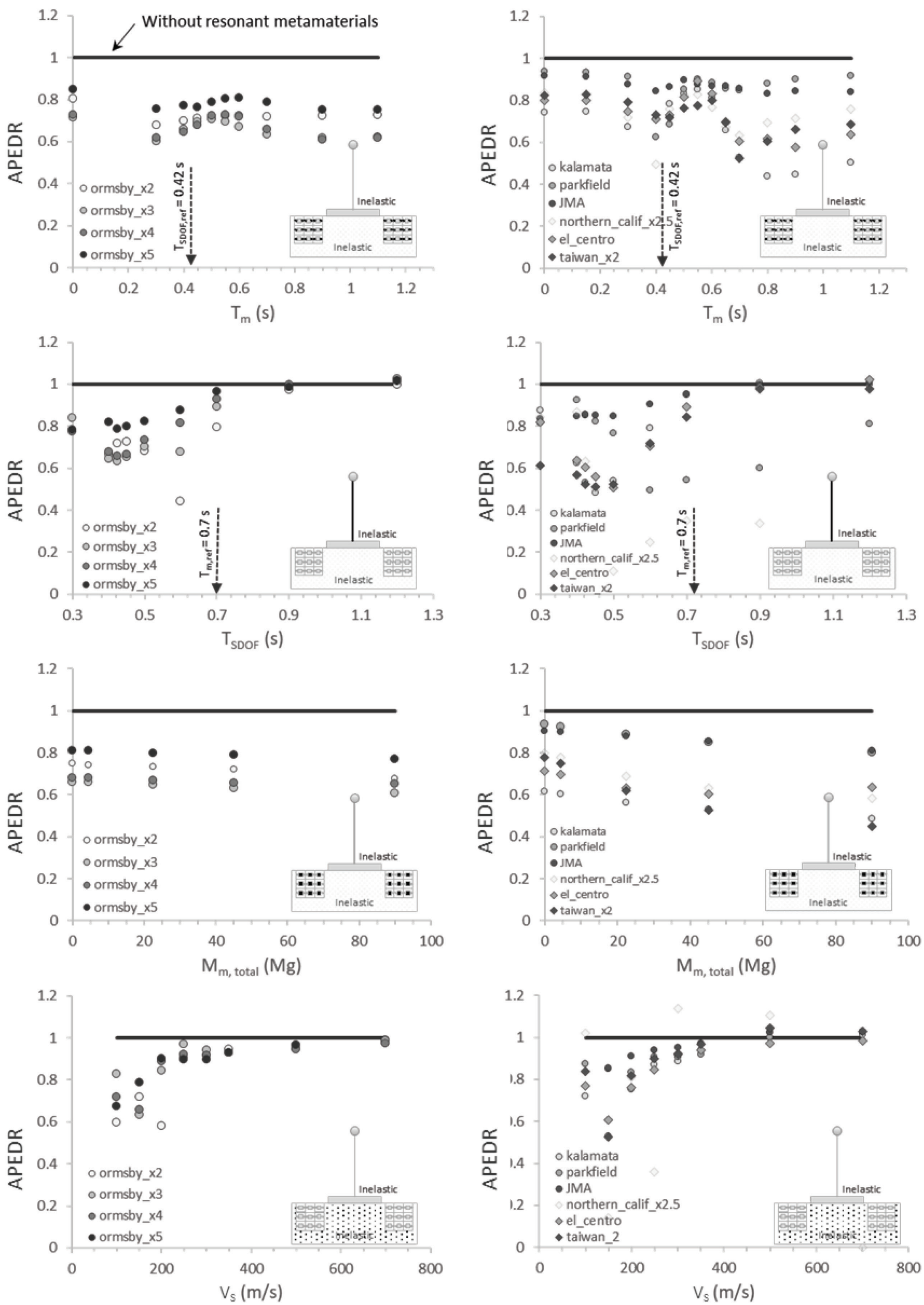

Fig. 15. (a) Nonlinear structure on nonlinear soil parametric analysis: effect of investigated parameters on $APEDR$. $APEDR$ < 1 corresponds to a beneficial effect of the metamaterials, while $APEDR$ > 1 to a detrimental effect.

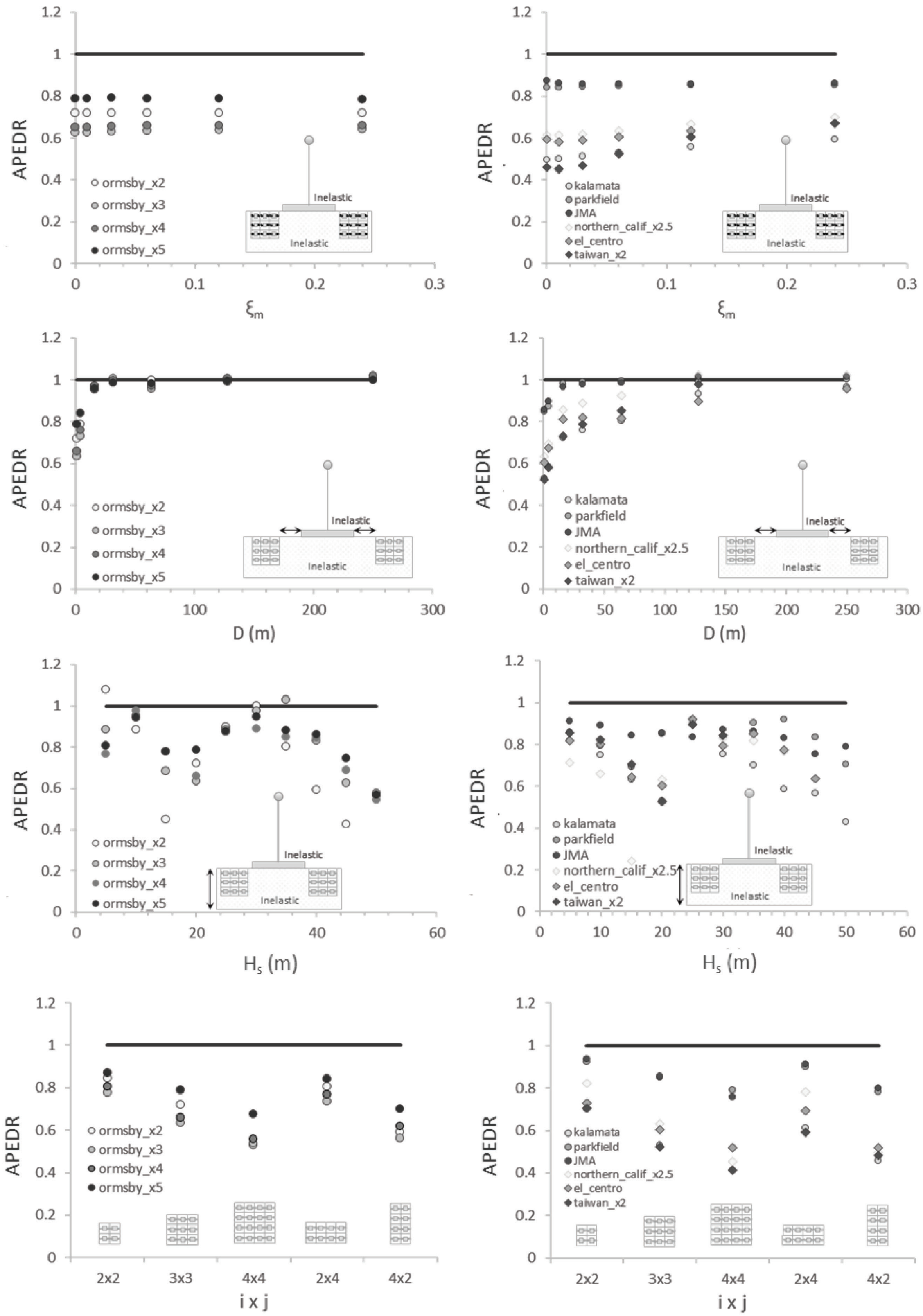

Fig. 16. (b) Nonlinear structure on nonlinear soil parametric analysis: effect of investigated parameters on $APEDR$. $APEDR$ < 1 corresponds to a beneficial effect of the metamaterials, while $APEDR$ > 1 to a detrimental effect.

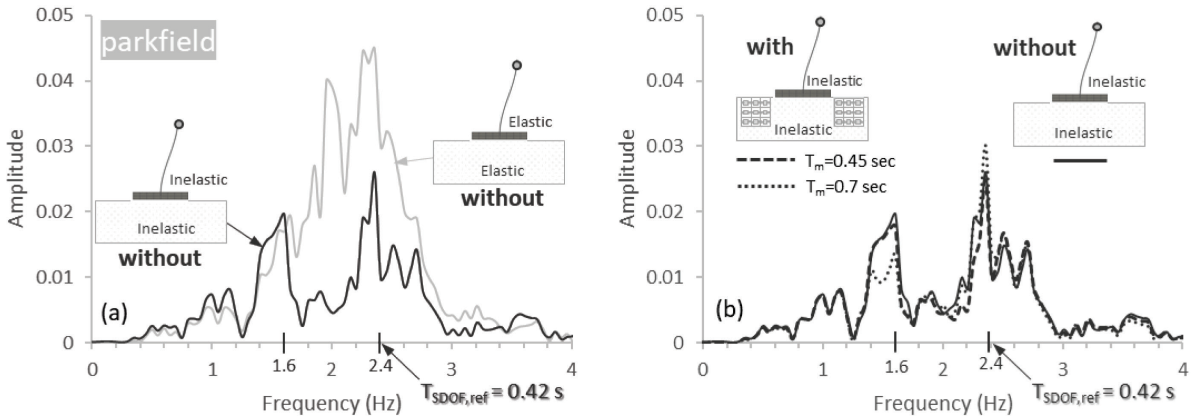

Fig. 17. Fourier spectra of the SDOF system top node acceleration time history excited by the 2004 Parkfield earthquake. Comparison of: (a) elastic and inelastic unprotected ("without") reference case; and (b) inelastic unprotected ("without") reference case to two protected ("with") cases (T_m = 0.45 and 0.7 s).

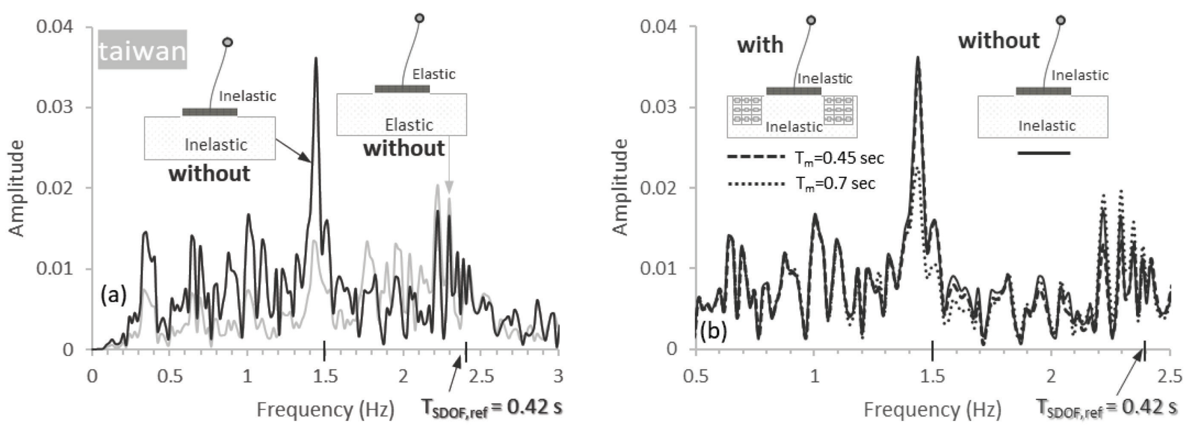

Fig. 18. Fourier spectra of the SDOF system top node acceleration time history excited by the 1986 Taiwan earthquake. Comparison of: (a) elastic and inelastic unprotected ("without") reference case; and (b) inelastic unprotected ("without") reference case to two protected ("with") cases (T_m = 0.45 and 0.7 s).

Of great interest are the energy dissipation results obtained from the variation of the total oscillating mass $M_{m,total}$. For $M_{m,total}$ = 0 (empty unit cells), the energy reduction mechanism (the "shadow" effect, related only to the kinematic and not to the inertial interaction between the unit cells and the surrounding soil) that was observed for elastic soil to be of minor significance, now becomes at least equally important as the main resonance-based reduction mechanism (i.e., the out-of-phase oscillation of the internal masses), which is related to the inertial interaction between the unit cells and the soil. This simply means that just the mere presence of stiff empty boxes in the surrounding soil, right next to the structure, leads to a reduction of its response up to some extent. The reason this kinematic-interaction-related mechanism is more pronounced for inelastic soil conditions is attributed to the decrease of the seismic wavelengths due to nonlinear soil response. As the wavelengths of vertically propagating shear waves are getting smaller (since the secant stiffness of the soil decreases), they become comparable with the embedment depth of the metamaterials, thus enhancing the beneficial effect of kinematic interaction.

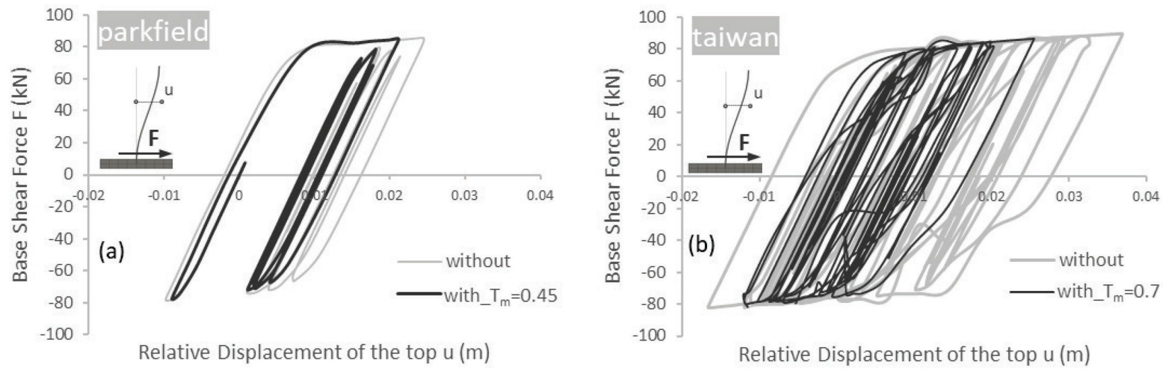

Fig. 19. Base shear–drift $(F - \delta)$ response of the SDOF system subjected to: (a) the 2004 Parkfield; and (b) the 1986 Taiwan earthquake. Comparison of the inelastic "without" reference cases to the inelastic "with" cases with T_m = 0.45 s and T_m = 0.7 s for the 2004 Parkfield and 1986 Taiwan earthquakes, respectively.

To visually explain this interesting outcome, the total plastic strain magnitude contours in the soil are plotted for the unprotected ("without") case (**Fig. 19a**) and for metamaterials of $M_{m,total}$ = 0 (i.e., empty boxes, **Fig. 19b**) for the 1986 Kalamata excitation. This comparison clearly reveals the aforementioned "shadow" effect. It is visible that for the case of the unprotected SDOF system, plastic strains are developed beneath it. However, thanks to the kinematic interaction, the addition of empty unit cells can be seen to create a protective "shadow" zone in the vicinity of the structure, shielding it from incoming seismic waves. For a given vertically propagating wavefield, such beneficial kinematic interaction effect is expected to diminish with the decrease of the embedment depth of the unit cell. **Figure 19c** shows exactly that: the 2x4 arrangement of empty unit cells creates a smaller protective zone compared to the one of the 3x3 case. In terms of $APEDR$, the results are 0.62 and 0.72 for the 3x3 and 2x4 cases, respectively. It should be noted, though, that a pronounced kinematic interaction between the empty unit cells and the vertically propagating shear waves (with wavelengths of similar size to metamaterials embedment depth) does not guarantee a reduction in structure response.

For this to happen, the excitation period of the incoming waves should be close to the resonant period of the SDOF system. This is characteristically shown in **Fig. 20a**, which investigates the effect of T_{SDOF} (every other parameter being constant) for $M_{m,total}$ = 0. As the natural period of the SDOF system decreases, the beneficial effect of the empty unit cells in decreasing the response of the SDOF system is increased. This is again attributed: (a) to the similar size of wavelengths compared to the metamaterials embedment depth; and (b) to the fact that the period that corresponds to these wavelengths is close to the shorter natural periods of the SDOF system (T_{SDOF} < 0.5 s). For structures with longer natural periods, the beneficial effect of the empty boxes is only marginal. The long period waves (that match the natural period of the SDOF system) also have long wavelengths ($V_S = \lambda / T$). As a result, the size of the empty boxes becomes too small to affect the longer period inciting waves.

Finally, **Fig. 20b** shows the influence of the unit cell Young's modulus, $E_{unit\ cell}$, for $M_{m,total}$ = 0 (empty unit cells). As expected, for stiff unit cells, $E_{unit\ cell}$ > 25 GPa (which corresponds to reinforced concrete), there is practically no influence on the results, suggesting that reinforced concrete can provide the required rigidity, and could be used as the construction material of the unit cells.

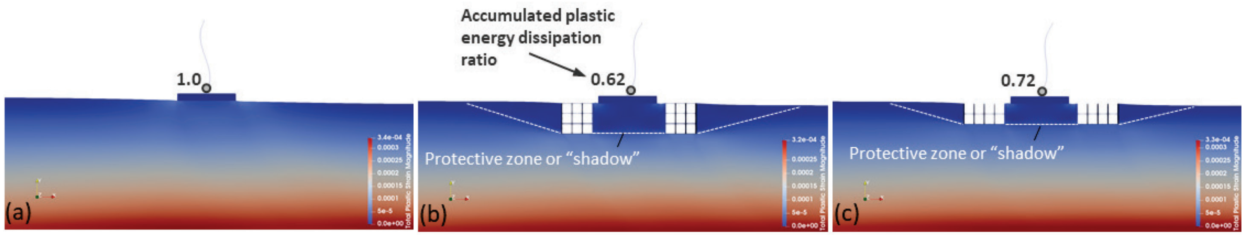

Fig. 20. Contours of total plastic strain magnitude in the soil at the same time step (t=4s) during the 1986 Kalamata earthquake for: (a) unprotected reference case; (b) 3x3, empty unit cells; and (c) 2x4, empty unit cells.

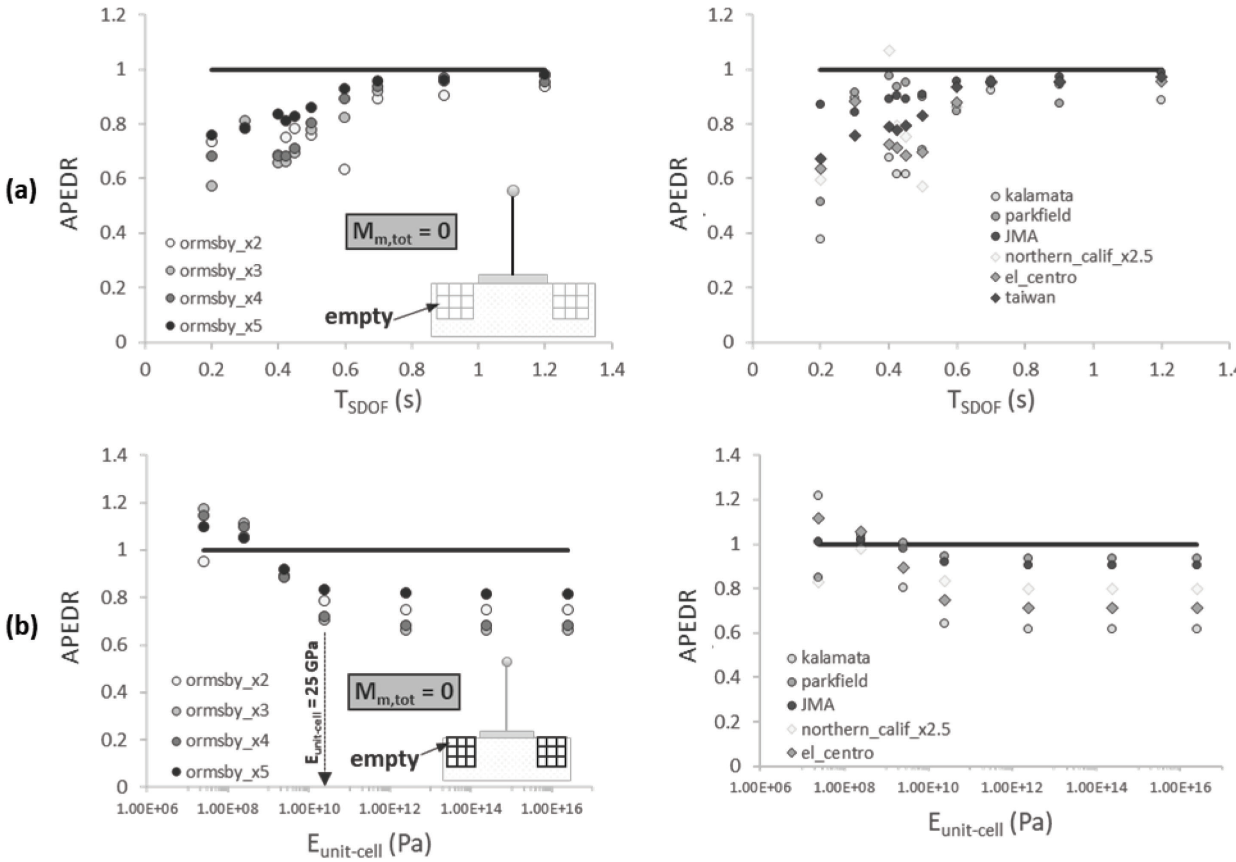

Fig. 20. Nonlinear structure on nonlinear soil protected with empty unit cells, $M_{m,total}$ = 0. The effect on $APEDR$ of: (a) the natural period T_{SDOF} of the structure; and (b) the unit cell Young's modulus $E_{unit\ cell}$.

The effect of the small-strain stiffness of the soil, or equivalently of its shear wave velocity V_S, is investigated next (**Fig. 15a**). The trends are quite similar to those observed previously for elastic soil, suggesting that the metamaterials are more effective for softer soil. Thus, the previously discussed expectation that the metamaterials would be beneficial in stiffer but inelastic soils, that could potentially yield and soften, did not materialize. The increase of stiffness is in proportion to the undrained shear strength (G_0 = 1000 S_u), and therefore yielding requires proportionally larger shear stresses. Although the developing shear stresses are a function of soil response, which is in turn, a function of G_0, this implies that the softening due to soil yielding is less pronounced than anticipated. Still though, the effectiveness of resonant metamaterials could increase for larger G_0/S_u ratios.

The damping ratio ξ_m of the resonant metamaterials seems to be of less importance (**Fig. 15b**). For most of the excitations, the results are more or less unaffected by the variation of ξ_m. However, in quite a few cases, the trend that was observed previously for elastic soil is observed: the resonant metamaterials become less effective for higher damping ratios ξ_m.

Looking at the effect of the distance D between the unit cells and the SDOF system, the previously discussed hypothesis is confirmed. No amplification effects are noticed in **Fig. 15b**, as the waves generated from the oscillation of the internal masses fade out due to soil inelasticity, before making their way back to the SDOF system. Another important conclusion is the very localized effect that resonant metamaterials have, which implies that their major influence on structural response vanishes when they are placed only a few meters away (D > 15 m). In combination with the previously discussed effect of T_{SDOF} (**Fig. 15a**), where no amplifications were observed, this may indicate that resonant metamaterials pose no threat to nearby structures.

The next investigated parameter is the soil depth H_s. As shown in **Fig. 15b**, an almost linear decrease of the plastic dissipation ratio is noticed from H_s = 5 to 20 m, and then from H_s = 20 to 50 m, with a jump in-between. These variations are mainly attributed to the modifications of the input motion target on the soil surface due to different soil depths, in combination with soil inelasticity. It is reminded that in the current study the effective forces of the DRM create a wave field that gives exactly the targeted acceleration time history at the desired depth, provided that the soil layers are linear elastic. With soil inelasticity, the incoming waves are filtered accordingly, resulting in slightly different—in amplitude and frequency content—acceleration time history, depending on the degree of inelasticity. Thus, if the resulting input motion at the base of the SDOF system has a frequency content that encompasses the resonant frequency of the SDOF system, the latter will oscillate with this frequency, which the resonant metamaterials are designed to protect (e.g., for H_s = 20 m). However, if the frequency content of the input motion does not include the resonant frequency of the SDOF system, the latter is forced to oscillate at other frequencies, where metamaterials are not optimally tuned, resulting in a drop of their efficiency (e.g., for H_s = 25 m).

The last investigated parameter is the geometric configuration of the metamaterials (number of rows i and columns j). Evidently, as the embedment depth of the metamaterials increases (from 2x2 to 3x3 to 4x4, and from 2x4 to 4x2), their size tends to approach the incoming wavelengths, which leads to more pronounced kinematic interaction with the soil, and thus to a reduction of $APEDR$.

7. Conclusions

A thorough 2D parametric analysis was conducted using the finite element method to evaluate the efficiency of resonant metamaterials (multiple unit cells embedded in the soil, with horizontally vibrating internal masses) as a seismic risk mitigation method for nonlinear structures, excited by shear waves vertically propagating through nonlinear soil. Linear-elastic conditions for the soil and the structure (represented by a SDOF system) were also investigated, to identify the key mechanisms governing the interactions with the resonant metamaterials. The key conclusions are summarized as follows:

- Two main protective mechanisms of the resonant metamaterials for the structure were identified. The first one is related to inertial interaction between the resonant metamaterials and the surrounding soil. The reduction in the acceleration response of the surrounding soil, and consequently of the structure, is driven by the out-of-phase oscillation of the resonating unit cell masses relative to the oscillation of the surrounding soil, for excitation periods close to the resonance of the SDOF system. In addition, the greater the oscillation amplitude of the masses during the out-of-phase oscillation, the larger the reduction in structural response. The second mechanism (the so-called "shadow" effect) is related to kinematic interaction between the metamaterials and the surrounding soil, and was revealed to its full extent in the analysis of empty unit cells (zero oscillating masses). For this mechanism to become beneficial for structure, two conditions should be satisfied simultaneously: (a) the embedment depth of the metamaterials should be comparable to the wavelengths of the incoming vertically propagating seismic waves (to activate kinematic interaction); and (b) the period of those waves should be close to the natural period of the structure.

- For the elastic SDOF system, the maximum response reduction can be achieved for natural period of the resonant metamaterials T_m equal or a bit larger than the period of the structure T_{SDOF} , so as to ensure the out-of-phase oscillation of the metamaterials with the surrounding soil at excitation periods close to T_{SDOF} . For the inelastic structure, T_m should be equal or a bit larger than the expected effective elongated period of the structure, due to its inelastic behaviour. Therefore, in the case of nonlinear structural response, tuning of the metamaterials for all possible seismic scenarios is not possible, calling for optimization and reasonable compromises.
- In the case of soil and structural inelasticity, no response amplification effects due to the presence of resonant metamaterials was observed. Moreover, the effect of resonant metamaterials on structural response was shown to rapidly decrease with the increase of their distance from the structure. This indicates that resonant metamaterials do not pose a threat to nearby structures, and could therefore be deployed as a means of seismic protection.
- If properly tuned, the efficiency of resonant metamaterials increases with a rational increase of the oscillating masses (up to the mass of the SDOF system).
- In general, the efficiency of resonant metamaterials increases as the soil becomes softer. For stiffer soils (V_S > 350 m/s), the beneficial effects of resonant metamaterials diminish.
- The Ormsby wavelet, with constant amplitude for the elastic parametric analyses, and gradually increasing amplitude for the inelastic ones, reproduced quite satisfactorily most of the trends observed with the real seismic motions.
- Potential limitations of the investigated resonant metamaterials could be the relatively large number and quantity of vibrating masses (approaching in total the mass of the SDOF system) that is required to increase the metamaterial efficiency, and the fact that for stiff soils (V_S > 350 m/s) the resonant metamaterial mechanism has practically no appreciable effects on structural response.

Acknowledgment

This research was part of the project 'Inspire' funded by the European Union's Horizon 2020 research and innovation programme under the Marie Skłodowska-Curie grant agreement no. 813424. Additional support from ETH Zurich and University of California Davis is gratefully acknowledged.

References

[1] Barkan DD. Dynamics of bases and foundations. McGraw-Hill Companies; 1962.

[2] Woods RD. Woods - Screening of surface waves in soils.pdf. J Soil Mech Found Div 1968;94:951–79.

[3] Segol G, Lee PCY, Abel JF. Amplitude Reduction of Surface Waves by Trenches. J Eng Mech Div 1978;104:621–41.

[4] Avilev J, Sanchez-Sesma FJ. Piles as Barriers for Elastic Waves. J Geotech Engrg 1983;109:1133–46.

[5] Pendry JB, Schurig D, Smith DR. Controlling electromagnetic fields. Science (80-) 2006;312:1780–2. https://doi.org/10.1126/science.1125907.

[6] Tsakmakidis KL, Boardman AD, Hess O. "Trapped rainbow" storage of light in metamaterials. Nature 2007;450:397–401. https://doi.org/10.1038/nature06285.

[7] Craster R V, Guenneau S. Acoustic metamaterials: Negative refraction, imaging, lensing and cloaking. vol. 166. 2012.

[8] Aguzzi G, Kanellopoulos C, Wiltshaw R, Craster R V., Chatzi EN, Colombi A. Octet lattice-based plate for elastic wave control. Sci Rep 2022;12:1088. https://doi.org/10.1038/s41598-022-04900-0.

[9] Colombi A, Roux P, Guenneau S, Gueguen P, Craster R V. Forests as a natural seismic metamaterial: Rayleigh wave bandgaps induced by local resonances. Sci Rep 2016;6:1–7. https://doi.org/10.1038/srep19238.

[10] Colombi A, Colquitt D, Roux P, Guenneau S, Craster R V. A seismic metamaterial: The resonant metawedge. Sci Rep 2016;6:1–6. https://doi.org/10.1038/srep27717.

[11] Roux P, Bindi D, Boxberger T, Colombi A, Cotton F, Douste-Bacque I, et al. Toward seismic metamaterials: The METAFORET project. Seismol Res Lett 2018;89:582–93. https://doi.org/10.1785/0220170196.

[12] La Salandra V, Wenzel M, Bursi OS, Carta G, Movchan AB. Conception of a 3D metamaterial-based foundation for static and seismic protection of fuel storage tanks. Front Mater 2017;4:1–13. https://doi.org/10.3389/fmats.2017.00030.

[13] Basone F, Wenzel M, Bursi OS, Fossetti M. Finite locally resonant Metafoundations for the seismic protection of fuel storage tanks. Earthq Eng Struct Dyn 2019;48:232–52. https://doi.org/10.1002/eqe.3134.

[14] Sun F, Xiao L, Bursi OS. Optimal design and novel configuration of a locally resonant periodic foundation (LRPF) for seismic protection of fuel storage tanks. Eng Struct 2019;189:147–56. https://doi.org/10.1016/j.engstruct.2019.03.072.

[15] Franchini A, Bursi OS, Basone F, Sun F. Finite locally resonant metafoundations for the protection of slender storage tanks against vertical ground accelerations. Smart Mater Struct 2020;29. https://doi.org/10.1088/1361-665X/ab7e1d.

[16] Sun F, Xiao L, Bursi OS. Quantification of seismic mitigation performance of periodic foundations with soil-structure interaction. Soil Dyn Earthq Eng 2020;132. https://doi.org/10.1016/j.soildyn.2020.106089.

[17] Miniaci M, Krushynska A, Bosia F, Pugno NM. Large scale mechanical metamaterials as seismic shields. New J Phys 2016;18. https://doi.org/10.1088/1367-2630/18/8/083041.

[18] Krödel S, Thomé N, Daraio C. Wide band-gap seismic metastructures. Extrem Mech Lett 2015;4:111–7. https://doi.org/10.1016/j.eml.2015.05.004.

[19] Zaccherini R, Palermo A, Marzani A, Colombi A, Dertimanis V, Chatzi E. Mitigation of Rayleigh-like waves in granular media via multi-layer resonant metabarriers. Appl Phys Lett 2020;117:1–6. https://doi.org/10.1063/5.0031113.

[20] Palermo A, Vitali M, Marzani A. Metabarriers with multi-mass locally resonating units for broad band Rayleigh waves attenuation. Soil Dyn Earthq Eng 2018;113:265–77. https://doi.org/10.1016/j.soildyn.2018.05.035.

[21] Colombi A, Zaccherini R, Aguzzi G, Palermo A, Chatzi E. Mitigation of seismic waves: Metabarriers and metafoundations bench tested. J Sound Vib 2020;485:115537. https://doi.org/10.1016/j.jsv.2020.115537.

[22] Zaccherini R, Colombi A, Palermo A, Dertimanis VK, Marzani A, Thomsen HR, et al. Locally Resonant Metasurfaces for Shear Waves in Granular Media. Phys Rev Appl 2020;13:1–10. https://doi.org/10.1103/PhysRevApplied.13.034055.

[23] Cacciola P, Tombari A. Vibrating barrier: A novel device for the passive control of structures under ground motion. Proc R Soc A Math Phys Eng Sci 2015;471. https://doi.org/10.1098/rspa.2015.0075.

[24] Geuzaine C, Remacle J-F. Gmsh: A 3-D finite element mesh generator with built-in pre-and post-processing facilities. Int J Numer Methods Eng 2009;79:1309–31.

[25] Jeremic B, Jie G, Cheng Z, Tafazzoli N, Tasiopoulou P, Pisano F, et al. The Real ESSI Simulator System. Univ California, Davis 2022.

[26] Bielak J, Loukakis K, Hisada Y, Yoshimura C. Domain reduction method for three-dimensional earthquake modeling in localized regions, part I: Theory. Bull Seismol Soc Am 2003;93:817–24. https://doi.org/10.1785/0120010251.

[27] Yoshimura C, Bielak J, Hisada Y, Fernández A. Domain reduction method for three-dimensional earthquake modeling in localized regions, part II: Verification and applications. Bull Seismol Soc Am 2003;93:825–40. https://doi.org/10.1785/0120010252.

[28] Jeremić B, Jie G, Preisig M, Tafazzoli N. Time domain simulation of soil-foundation-structure interaction in non-uniform soils. Earthq Eng Struct Dyn 2009;38:699–718.

[29] Abell JA, Orbović N, McCallen DB, Jeremic B. Earthquake soil-structure interaction of nuclear power plants, differences in response to 3-D, 3 × 1-D, and 1-D excitations. Earthq Eng Struct Dyn 2018;47:1478–95. https://doi.org/10.1002/eqe.3026.

[30] Wang H, Yang H, Feng Y, Jeremić B. Modeling and simulation of earthquake soil structure interaction excited by inclined seismic waves. Soil Dyn Earthq Eng 2021;146. https://doi.org/10.1016/j.soildyn.2021.106720.

[31] Zhang W, Seylabi EE, Taciroglu E. An ABAQUS toolbox for soil-structure interaction analysis. Comput Geotech 2019;114. https://doi.org/10.1016/j.compgeo.2019.103143.

[32] Zhang W, Taciroglu E. 3D time-domain nonlinear analysis of soil-structure systems subjected to obliquely incident SV waves in layered soil media. Earthq Eng Struct Dyn 2021;50:2156–73. https://doi.org/10.1002/eqe.3443.

[33] Thomson WT. Transmission of elastic waves through a stratified solid medium. J Appl Phys

1950;21:89–93. https://doi.org/10.1063/1.1699629.

[34] Haskell NA. The dispersion of surface waves on multilayered media. Bull Seismol Soc Am 1953;43:17–34.

[35] Spacone E, Filippou FC, Taucer FF. Fibre beam--column model for non-linear analysis of R/C frames: Part I. Formulation. Earthq Eng Struct Dyn 1996;25:711–25.

[36] Menegotto M, Pinto PE. Method of Analysis for Cyclically Loaded R. C. Plane Frames Including Changes in Geometry and Non-Elastic Behavior of Elements under Combined Normal Force and Bending. Proc IABSE Symp Resist Ultim Deform Struct Acted by Well Defin Loads 1973:15–22.

[37] Filippou FC, Popov EP, Bertero VV. Effects of bond deterioration on hysteretic behavior of reinforced concrete joints 1983.

[38] Jeremić B, Yang Z, Cheng Z, Jie G, Tafazzoli N, Preisig M, et al. Nonlinear finite elements: Modeling and simulation of earthquakes, soils, structures and their interaction. Univ. California, Davis, CA, USA, Lawrence Berkeley Natl. Lab. Berkeley, CA, USA, 1989-2022. ISBN 978-0-692-19875-9, 2022.

[39] Eurocode 8: Design of structures for earthquake resistance-part 1: general rules, seismic actions and rules for buildings. Brussels Eur Comm Stand 2005.

[40] Manfredi G. Evaluation of seismic energy demand. Earthq Eng Struct Dyn 2001;30:485–99. https://doi.org/10.1002/eqe.17.

[41] Yang H, Feng Y, Wang H, Jeremić B. Energy dissipation analysis for inelastic reinforced concrete and steel beam-columns. Eng Struct 2019;197. https://doi.org/10.1016/j.engstruct.2019.109431.

[42] Yang H, Sinha SK, Feng Y, McCallen DB, Jeremić B. Energy dissipation analysis of elastic–plastic materials. Comput Methods Appl Mech Eng 2018;331:309–26. https://doi.org/10.1016/j.cma.2017.11.009.

[43] Anastasopoulos I, Gazetas G, Loli M, Apostolou M, Gerolymos N. Soil failure can be used for seismic protection of structures. Bull Earthq Eng 2010;8:309–26. https://doi.org/10.1007/s10518-009-9145-2.

[44] Kanellopoulos K, Gazetas G. Vertical static and dynamic pile-to-pile interaction in non-linear soil. Geotechnique 2020;70:432–47. https://doi.org/10.1680/jgeot.18.P.303.

[45] Radhima J, Kanellopoulos K, Gazetas G. Static and dynamic lateral non-linear pile–soil–pile interaction. Géotechnique 2021:1–16. https://doi.org/10.1680/jgeot.20.p.250.

[46] Frederick CO, Armstrong PJ. A mathematical representation of the multiaxial Bauschinger effect. Mater High Temp 2007;24:1–26. https://doi.org/10.1179/096034007X207589.

[47] Yang H, Wang H, Jeremić B. An Energy-Based Analysis Framework for Soil Structure Interaction Systems. Comput Struct 2022;In Print.

[48] Vucetic M, Dobry R. Effect of soil plasticity on cyclic response. J Geotech Eng 1991;117:89–107.

[49] Yang H, Wang H, Feng Y, Wang F, Jeremić B. Energy dissipation in solids due to material inelasticity, viscous coupling, and algorithmic damping. J Eng Mech 2020;145. https://doi.org/https://doi.org/10.1061/(ASCE)EM.1943-7889.0001617.